A RADIAL SCALE UP OF MATRIX ACIDIZING IN CARBONATE RESERVOIRS

A Thesis

by

SAMUEL LAUDON

Submitted to the Office of Graduate and Professional Studies of
Texas A&M University
in partial fulfillment of the requirements for the degree of

MASTER OF SCIENCE

Chair of Committee,	Alfred Daniel Hill
Committee Members,	Ding Zhu
	Victor M. Ugaz
Head of Department,	Jeff Spath

August 2021

Major Subject: Petroleum Engineering

ABSTRACT

Acidizing is a common technique used in completing wells in carbonate reservoirs to reduce skin factor. Generally, HCl is pumped into the formation where it will react with calcite and dolomite in the carbonate rock. The dissolved volumes are called wormholes because they look like tunnels through the rock. The wormholes must extend past the damage zone to be as effective as possible. At low injection rates, the wormholes are extremely inefficient because they have a large diameter but not a long-propagated distance into the formation. As injection rates increase for the same volume of pumped acid, the diameter decreases, and the wormhole length increases up to an optimal value.

The majority of research completed in this area is done on linear core floods due to the simplicity of the experiments. Linear core floods consist of flowing acid in a single direction through a small cylindrical core from one end to the other. The majority of the experiments are done to determine the optimal acid flux for a certain formation or acid type by measuring the amount of acid required to break through the core. More recent studies have shown that linear core floods do not accurately predict optimal values when pumping acid in the field. Radial acidizing floods can bridge the gap to more accurately represent field conditions.

This study consisted of radially flowing acid through a block of Indiana limestone that measured 4 feet by 4 feet by 3 feet where the shortest length was the height. A small 2-inch wellbore was drilled through the center of the block with a 1-inch diameter open hole completion. The acid flux used for this experiment was calculated using a global wormhole model fitted for radial flow. Acid was pumped through the wellbore until breakthrough was seen by the appearance of bubbles exiting the side of the block.

ACKNOWLEDGEMENTS

I would like to thank my parents for their continuous support and encouragement throughout this journey.

I would like to thank Dr. Hill and Dr. Zhu for their guidance during my time at Texas A&M and for the materials and funding to make this research possible.

Lastly, I would like to thank John Maldonado for his constant help in our project and in our department. He went above and beyond the job description to aid in our research and our equipment design.

CONTRIBUTORS AND FUNDING SOURCES

This work was supported by a committee involving my advisor, Dr. Dan Hill, along with Dr. Ding Zhu and Dr. Victor Ugaz.

The experiment was performed with the assistance of Juan Fernandez. All other work for this thesis was completed by the student independently.

This research was funded by the ASRP group consisting of Chevron, ConocoPhillips, Fluid Energy, Schlumberger, and Total.

The contents of this study are solely the responsibility of the author and do not necessarily represent the official views of the ASRP group.

NOMENCLATURE

A	Area, ft^2.
a_z	Wormhole axial spacing, unitless.
B	Compact dissolution regime correction to v_i, unitless.
d	General diameter, cm.
d_A	Diameter of core A, cm.
d_B	Diameter of core B, cm.
d_{core}	Diameter of core, cm.
$d_{e,wh}$	Wormhole diameter, cm.
d_{rep1}	Representative diameter parameter for $PV_{bt,opt}$, cm.
d_{rep2}	Representative diameter parameter for $v_{i,opt}$, cm.
d_{s1}	Diameter scale for $PV_{bt,opt}$, unitless.
d_{s2}	Diameter scale for $v_{i,opt}$, unitless.
f_1	Scaling factor used for $PV_{bt,opt}$, unitless.
f_2	Scaling factor used for $v_{i,opt}$, unitless.
h	Reservoir thickness, ft.
L_{core}	Length of the core, ft.
L_{rep1}	Representative length used for $PV_{bt,opt}$, ft.
L_{rep2}	Representative length used for $v_{i,opt}$, ft.
l_{wh}	Length of the wormhole, ft.
m_{wh}	Number of dominant wormholes along the angular direction, unitless.
N_{Ac}	Acid capacity number, unitless.
PV_{bt}	Pore volumes to breakthrough, unitless.
$PV_{bt,opt}$	Optimal pore volumes to breakthrough, unitless.

$PV_{bt,opt,A}$	Optimal pore volumes to breakthrough for a core of A diameter, unitless.
$PV_{bt,opt,B}$	Optimal pore volumes to breakthrough for a core of B diameter, unitless.
$PV_{bt,opt,core}$	Optimal pore volumes to breakthrough for a core, unitless.
q	Flow rate, mL/min.
q_{perf}	Flow rate through a perforation, mL/min.
r_w	Wellbore radius, ft.
r_{wh}	Wormhole radius, ft.
$r_{wh,rep1}$	Representative wormhole length for $PV_{bt,opt}$, ft.
$r_{wh,rep2}$	Representative wormhole length for $v_{i,opt}$, ft.
t	Time, min.
V	Volume of acid, L.
v_i	Interstitial velocity, cm/min.
$v_{i,opt}$	Optimal interstitial velocity, cm/min.
$v_{i,opt,A}$	Optimal interstitial velocity for core A, cm/min.
$v_{i,opt,B}$	Optimal interstitial velocity for core B, cm/min.
$v_{i,opt,core}$	Optimal interstitial velocity for a general core, cm/min.
$v_{i,tip}$	Interstitial velocity at the tip of the wormhole, cm/min.
v_{wh}	Wormhole velocity, ft/min.
W_b	Constant used in the Buijse and Glasbergen (2005) model, $(cm/min)^{-2}$.
W_{eff}	Constant used in the Buijse and Glasbergen (2005) model, $(cm/min)^{1/3}$.
γ	Exponent used in the Buijse and Glasbergen (2005) model, unitless.
ε_1	Exponent relating decrease in $PV_{bt,opt}$ as scale increases in the Schwalbert (2019) model, unitless.

ε_2	Exponent relating decrease in $v_{i,opt}$ as scale increases in the Schwalbert (2019) model, unitless.
π	Mathematical operator pi, unitless.
ϕ	Porosity, unitless.

TABLE OF CONTENTS

Page

LIST OF FIGURES

Page

LIST OF TABLES

Page

1. INTRODUCTION AND OBJECTIVES

1.1 Introduction

Acidizing jobs are done to create wormholes that extend past the damage zone and decrease the associated skin factor of a well. Acidizing is most commonly used in carbonate reservoirs due to the fast reaction of hydrochloric acid with calcite. Before taking new ideas to the field to test them on expensive wells, small scale research is necessary to ensure better success and cost effectiveness. Generally, this is done through linear core floods. The cores are cylindrical in shape and generally range from 1” to 4” in diameter and anywhere from 4” to 16” in length. Linear core floods are the simplest and cheapest method to understand how acid will affect a given formation along with giving information on how to improve acidizing techniques. The porosity of a core can be determined by first drying the core using an oven and taking a mass measurement. This is then followed by soaking the core in a vacuum sealed water chamber and then a second mass measurement is taken to determine the amount of water the core holds. Flowing water through the core can give values for permeability by assessing the pressures which are then in turn used to calculate reservoir properties. In addition to learning rock properties, core floods can also be used to find better acidizing methods such as acid type, acid temperature, and flow rate. In conjunction with this, there has been a growing interest in radial core floods where instead of flowing from one end of a core to another, acid flows outwardly in all directions.

1.2 Objectives

The objective of this research was to test radial matrix acidizing on a large block of Indiana limestone at the optimal interstitial velocity using hydrochloric acid. There are a lot of intermediate objectives to make the overall research a success that do not depend on the outcome of the experiment. Essentially those determine the correct way to run an experiment at this scale to create a baseline for future experiments. This includes the apparatus design, experimental procedure, wellbore design, data collection, and visualization of the wormholes created.

Pressure and flow rate data were collected during the experiment to compare with theoretical results given in various wormhole propagation models and determine their validity. In addition, CT scans were generated from the acidized rock to determine the pathway that the acid took during the experiment. These could be used in conjunction with a streamline simulation of water through a homogeneous block to show comparisons of the two pathways between the simulated homogeneous block and the physical block used in the experiment.

This experiment has the largest block used for radial matrix acidizing to date. The block is large enough to act in the same manner as a reservoir during a conventional acid job. With the apparatus created for this experiment, many other experiments can be completed in a shorter time frame. These studies can be used to create a wormhole efficiency chart by conducting various experiments at different interstitial velocities. Another study that could be done from this research is to conduct the experiment at reservoir temperatures to study acid behavior on a large scale as temperature is increased.

2. LITERATURE REVIEW

2.1 Linear Acidizing Models

With only 4 to 5 samples, a researcher can conduct multiple linear core floods to determine the optimal interstitial velocity telling operators exactly how to pump their acid jobs. This value will change based on the rock composition, reservoir temperature, acid type, completion type, and many more variables. This being said, there are almost an endless number of possibilities of optimal values hence the need for linear core floods. The first models created are very simplistic, and do not give as much usable information as later models.

The Volumetric model (Economides et al. 1994) assumes that the acid will dissolve the same percentage of rock as it propagates through the matrix, and is given as

$$r_{wh} = \sqrt{r_w^2 + \frac{V}{PV_{bt}\pi\phi h}} \tag{1}$$

where r_{wh} is the wormhole radius and PV_{bt} is the pore volume to breakthrough. Pore volume to breakthrough is the amount of acid needed in terms of the rock's pore volume to propagate a wormhole a certain distance. This can easily be done using linear core floods and measuring the amount of acid pumped with the differential pressure to note when breakthrough occurs. The pressure difference across the core will reduce to zero when breakthrough is achieved. This makes finding the breakthrough point very easy when visual inspection is not available due to the apparatus. The volume needed to propagate a certain distance is found easily with only a few known parameters which makes this model great for simple calculations. This concept will be introduced in the next model.

A semi empirical model (Buijse and Glasbergen, 2005) correlates the velocity of the wormholes to the pore volume to breakthrough using acid flux (interstitial velocity). They found that the two are inversely related. From there, they plotted pore volumes to breakthrough vs. interstitial velocity shown in Figure 1 along with wormhole velocity vs. interstitial velocity. They were then able to develop their correlation. It is given as

$$v_{wh} = W_{eff} {v_i}^{2/3} B(v_i) \tag{2}$$

$$B(v_i) = (1 - exp(-W_B {v_i}^2))^2 \tag{3}$$

$$PV_{bt} = \frac{v_i}{v_{wh}} = \frac{{v_i}^{1/3}}{W_{eff} B(v_i)} \tag{4}$$

$$W_{eff} = \frac{{v_{i-opt}}^{1/3}}{PV_{bt-opt}} \tag{5}$$

$$W_B = \frac{4}{{v_{i-opt}}^2} \tag{6}$$

These set of equations then simplify to the following

$$v_{wh} = \frac{dr_{wh}}{dt} = \left(\frac{v_i}{PV_{bt}}\right) \left(\frac{v_i}{v_{i,opt}}\right)^{-\gamma} (1 - exp(-4(\frac{v_i}{v_{i,opt}})^2)^2 \tag{7}$$

where v_{wh} is the wormhole velocity and v_i is the interstitial velocity (acid flux). The model they presented is not used as much today as other models have been proved to be more accurate. However, their methodology is still widely used. There is an optimal interstitial velocity for each rock matrix that will result in the lowest value for pore volume to breakthrough. This can be found by completing core floods for low and high velocities.

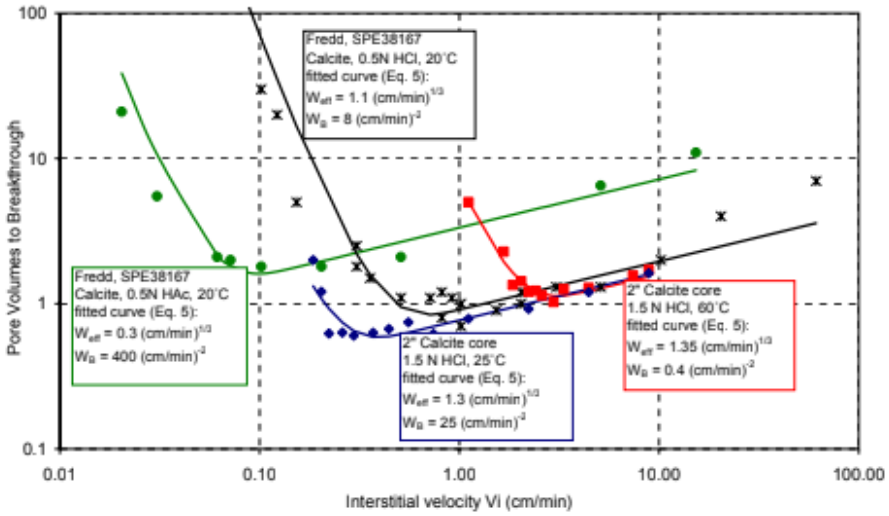

Figure 1. Wormhole efficiency chart (Buijse and Glasbergen, 2005)

Generally, it only takes 4-5 experiments to create an efficiency curve showing the optimal interstitial velocity. They made a workflow for the radial scenario in which a time step was used to calculate the acid flux, velocity, and wormhole radius for given times. This model works better for core samples, but as the size increases, the model is less accurate. This is why more accurate radial models exist. With that being said, almost all use the logic presented by Buijse and Glasbergen (2005).

2.2 Radial Acidizing Models

Radial matrix acidizing allows for more realistic experiments giving more usable data. These experiments allow flow in all directions to better simulate what is actually happening in a field scale acid completion. Unfortunately, they are more difficult to conduct due to the apparatus and size of the rock required. Thus, not many large block radial acidizing experiments had been completed until the last 10 years.

There were multiple studies completed in 2010, the first one completed by ExxonMobil (McDuff et al. 2010). Their work was on experimental scale up to a large block of carbonate rock, very similar to the project that was completed in this study. The largest block used in their experiment measured 14 ft^3 in volume, roughly 2.4 feet on each dimension. McDuff (2010) CT scanned the block after injection. The point in using a CT scanner is to see where the wormholes travelled during the experiment. A normal CT scanner could not be used in this application because they begin to lose resolution passed a certain distance in the rock, generally 6-8 inches. The scanner at the air force base was powerful enough to see 1 meter deep into the block. In their experiment, they applied pressure to the top and bottom of the rock to simulate reservoir conditions, and both were sealed off to force the acid to propagate horizontally as seen in Figure 2.

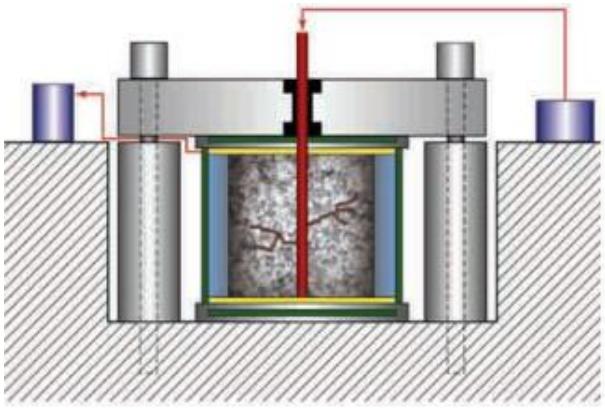

Figure 2. Sealed experimental chamber (McDuff et al. 2010)

The CT scans they produced were important in being able to see and understand how the wormholes propagate in radial acidizing. They noticed that almost all of the wormholes grew outward symmetrically. When they achieved breakthrough, there were many wormholes within an inch of breaking through in other parts of the rock.

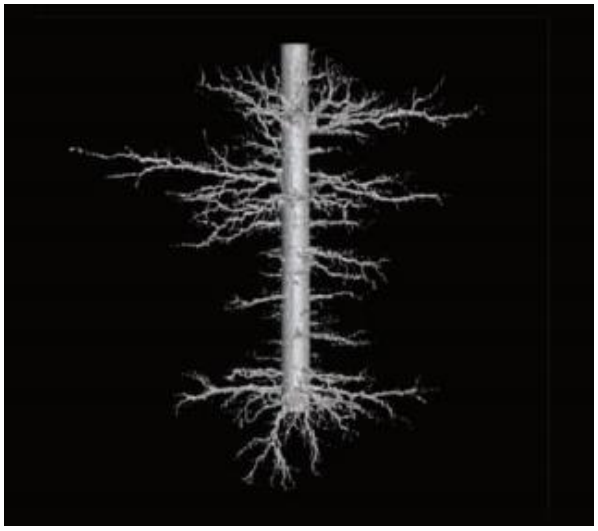

Figure 3. Radial CT scan (McDuff et al. 2010)

The second research in 2010 (Furui et al. 2010) focused on wormhole penetration in horizontal wells in carbonate reservoirs. Furui et al. (2010) thought there needed to be more extensive studies in this area because current models were not comprehensive enough and under-predicted acid stimulation effects. In detail, they tested the model by Buijse and Glasbergen (2005) and found that it was only effective in linear core floods. The predicted skin factor was above the actual skin factor proving the Buijse and Glasbergen (2005) model was under-predicting performance. The realization was that the optimal pore volume to breakthrough changed depending on the size of the core. This dependency was due to flow concentration at the wormhole tip along with boundary effects, and it caused larger diameter cores to be more efficient. They tested this in simulations of various core diameters where they kept track of the velocity at the tip of the dominating wormhole while holding injection rate constant. As predicted, the velocity at the tip was four times as great in a 4-inch core compared to a 1-inch core.

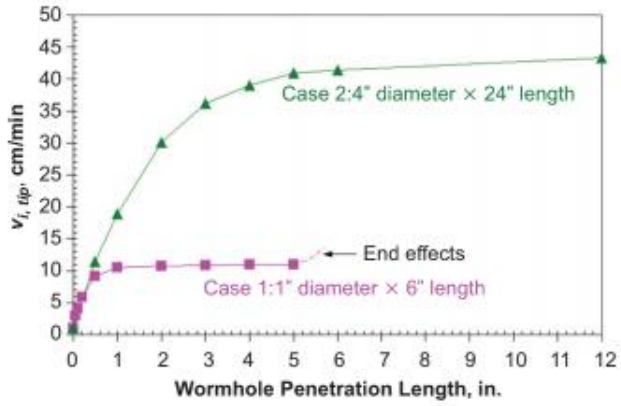

Figure 4. Comparison of core diameter (Furui et al. 2010)

The higher tip velocity explains why larger cores were more efficient in matrix acidizing results. A lower interstitial velocity could be used in larger cores to achieve the same wormhole propagation found in smaller diameter cores. Furui et al. (2010) took these results and applied them to the Buijse and Glasbergen (2005) model. The end equation is the following:

$$v_{wh} = v_{i,tip} N_{Ac} \left(\frac{v_{i,tip} PV_{bt,opt} N_{Ac}}{v_{i,opt}} \right)^{-\gamma} \{1 - exp[-4(\frac{v_{i,tip} PV_{bt,opt} N_{Ac} L_{core}}{v_{i,opt} r_{wh}})^2]\}^2 \quad (8)$$

where $v_{i,tip}$ is the interstitial velocity at the tip of the wormhole. The velocity equation varies depending on the flow geometry, but for radial flow it is given as:

$$v_{i,tip} = \frac{q}{\phi h \sqrt{\pi m_{wh}}} [(1 - a_z) \frac{1}{\sqrt{d_{e,wh} r_{wh}}} + a_z (\frac{1}{d_{e,wh}})] \quad (9)$$

The model was able to extend the work completed by Buijse and Glasbergen (2005) by refining their model to be more accurate for various core sizes.

Burton (2018) conducted several experiments to continue the work completed by Furui et al. (2010). From the linear core flood studies, it was found that pore volumes to breakthrough decrease as core size increases. The main reason for this phenomenon is there are fewer wormholes per unit volume. As they propagate, it will require less acid per unit volume to breakthrough in comparison to smaller diameters where the wormhole density is much greater. The pore volumes to breakthrough in 4-inch cores were four times smaller than those obtained from 1-inch cores (Burton 2018) confirming the work done by Furui et al. (2010).

In addition, radial experiments were conducted on two different sizes of carbonate blocks. The smaller size measured 14 inches in height and 10 inches in width while the larger size block measured 32 inches in height and 27 inches in width. Six tests were done on the smaller size, and only one test was done of the larger size block. The pore volumes to breakthrough averaged 0.04 for the smaller blocks, and the larger experiment yielded 0.03 (Burton 2018). The pore volumes to breakthrough found from field data were 0.03. All the radial experiments conducted by Burton (2018) replicated field pore volumes to breakthrough. Burton also compared experiments completed by Tardy (2007) and Qui (2018) and showed that both of their radial experiments resulted in higher pore volumes to breakthrough in the range of 0.09-0.15. The block used by Tardy (2007) had a height of 2.3 inches and a radius of 2.8 inches. The smaller dimensions could be why the pore volume to breakthrough values were higher.

The Schwalbert (2019) dissertation at Texas A&M focused on acid fracturing and matrix acidizing in carbonate reservoirs. His matrix acidizing research was based partially on experiments and partially on the Two-Scale Continuum model, a simulation technique that is not mentioned further in this literature. He used both methods to construct a new global matrix

acidizing model used for upscaling lab experiments to industry scale acidizing completions. The model is an updated version of the Furui et al. (2010) method that had expanded upon the Buijse and Glasbergen (2005) work. The first simple correlation he made is for the new values of optimal pore volumes to breakthrough and optimal interstitial velocity for changing diameters in linear floods.

$$PV_{bt,opt,B} = PV_{bt,opt,A}\left(\frac{d_A}{d_B}\right)^{\varepsilon_1} \tag{10}$$

$$v_{i,opt,B} = v_{i,opt,A}\left(\frac{d_A}{d_B}\right)^{\varepsilon_2} \tag{11}$$

One of the most important correlations in this study was the scale up model for optimal pore volumes to breakthrough and interstitial velocity. The upscaled parameters can be calculated by the following equations:

$$PV_{bt,opt}(d) = PV_{bt,opt,core}\left(\frac{d_{core}}{(d, d_{rep1})}\right)^{\varepsilon_1} \tag{12}$$

$$v_{i,opt}(d) = v_{i,opt,core}\left(\frac{d_{core}}{(d, d_{rep2})}\right)^{\varepsilon_2} \tag{13}$$

The d_{rep} is a representative value for the scale up. It will increase until the point in which efficiency does not increase as diameter or block size increases. He notes that for similar experiments d_{rep} and ε vary, and they may depend on rock mineralogy causing uncertainty in the model inputs. The Schwalbert (2019) global wormhole model is given as:

$$v_{wh} = \frac{dr_{wh}}{dt} = \left(\frac{v_i}{PV_{bt,opt,core} f_1}\right)\left(\frac{v_i}{v_{i,opt,core} f_2}\right)^{-\frac{1}{3}}\left(1 - exp\left(-4\left(\frac{v_i}{v_{i,opt,core} f_2}\right)^2\right)\right)^2 \quad (14)$$

$$f_1 = \left(\frac{d_{core}}{d_{s1}}\right)^{\varepsilon_1} \quad (15)$$

$$f_2 = \left(\frac{d_{core}}{d_{s2}}\right)^{\varepsilon_2} \quad (16)$$

The only difference between this model and the Buijse and Glasbergen (2005) model is the scaling factors f_1 and f_2 that are used in the wormhole velocity equation. He created two tables to solve for the required parameters in f_1 and f_2 for a given geometry and core size.

Linear Flow	Cylindrical Radial Flow	Spherical Flow
$v_{wh} = \frac{dl_{wh}}{dt}$	$v_{wh} = \frac{dr_{wh}}{dt}$	$v_{wh} = \frac{dR_{wh}}{dt}$
$\bar{v}_l = \frac{q}{\phi A}$	$\bar{v}_l = \frac{q}{\phi 2\pi L r_{wh}}$	$\bar{v}_l = \frac{q_{perf}}{\phi 4\pi R_{wh}^2}$
$d_{s1} = \min\left(\sqrt{\frac{4A}{\pi}}, d_{rep,1}\right)$	$d_{s1} = \sqrt{8\min(L, L_{rep,1})\min(r_{wh}, r_{wh,rep,1})}$	$d_{s1} = 4\min(R_{wh}, R_{wh,rep,1})$
$d_{s2} = \min\left(\sqrt{\frac{4A}{\pi}}, d_{rep,2}\right)$	$d_{s2} = \sqrt{8\min(L, L_{rep,2})\min(r_{wh}, r_{wh,rep,2})}$	$d_{s2} = 4\min(R_{wh}, R_{wh,rep,2})$

Table 1. Parameters for various geometries (Schwalbert 2019)

Parameter	Representative Value	Range Observed
ε_1	0.53	0.3 to 1
ε_2	0.63	0.6 to 1
$L_{rep,1}$	1 ft	0.7 ft to 1.5 ft
$r_{wh,rep,1}$	3 ft	0.7 ft to 10 ft
$L_{rep,2}$	1 ft	0.7 ft to 1.3 ft
$r_{wh,rep,2}$	1 ft	0.7 ft to 1.3 ft

Table 2. Representative values (Schwalbert 2019)

Schwalbert (2019) simplified the equations using the representative values for field scale. The scaling factors f_1 and f_2 can be shortened to:

$$f_1 = \left(\frac{d_{core}}{59}\right)^{\varepsilon_1} \tag{17}$$

$$f_2 = \left(\frac{d_{core}}{34}\right)^{\varepsilon_2} \tag{18}$$

The complete radial model is given as:

$$\frac{dr_{wh}}{dt} = \frac{\left(\frac{q}{\emptyset 2\pi L r_{wh}}\right)}{PV_{bt,opt,core}}\left[\frac{\sqrt{8\left(L, L_{rep1}\right)\left(r_{wh}, r_{wh,rep1}\right)}}{d_{core}}\right]^{\epsilon_1} X\left\{\frac{\left(\frac{q}{\emptyset 2\pi L r_{wh}}\right)}{v_{i,opt,core}}\left[\frac{\sqrt{8\left(L, L_{rep2}\right)\left(r_{wh}, r_{wh,rep2}\right)}}{d_{core}}\right]^{\epsilon_2}\right\}^{-\frac{1}{3}} X\left\{1 - exp\left\{-4\left\{\frac{\left(\frac{q}{\emptyset 2\pi L r_{wh}}\right)}{v_{i,opt,core}}\left[\frac{\sqrt{8\left(L, L_{rep2}\right)\left(r_{wh}, r_{wh,rep2}\right)}}{d_{core}}\right]^{\epsilon_2}\right\}^{2}\right\}\right\}^{2} \tag{19}$$

3. METHODOLOGY

3.1 Wellbore and Block Design

The block used for this experiment needed to be large enough to be considered field scale to use the representative values in the Schwalbert (2019) model, but small enough to fit inside the testing tank. Four blocks of the same size were purchased for cost effectiveness. Even though one block was used for this experiment, it made sense to purchase identical blocks for later experiments. The quarry that supplied the Indiana limestone blocks had a large piece and a saw already in their yard, so it did not require very much extra work on their part to get the blocks to the desired size. The fiberglass testing tank is 10 feet in diameter, so to get the most out of the allotted space, the block was cut to be 4 feet in length by 4 feet in width by 3 feet in height. The porosity and permeability values are 9.1% and 1 md respectively.

Figure 5. Indiana limestone blocks

The wellbore was meant to be simple and cost effective while sealing the annulus, holding pressure, and allowing a strong connection to the tubing connected to the pump. The

simplest way to design the wellbore was to have a 2-inch pipe sealed in the well with an open hole completion of 1 inch in diameter. With a height of 3 feet, the final decision was to have a 1 foot long open hole section in the middle of the block. To do that, the pipe had to reach 1 foot into the block, and then the bottom foot of the block will remain untouched. The pipe stuck out 6 inches from the block to make the connection to the tubing easier, meaning the pipe length was 18 inches long. Unfortunately, due to the size of the block, a conventional cement job was not an option. The simplest and most cost-effective solution was to use a high strength epoxy to glue the pipe in place by putting the epoxy on the pipe and shoving it down the wellbore. The epoxy used was J.B. Weld, and was rated to 5,000 psi. It came in two separate tubes, labeled A and B. When the tubes are mixed together they will immediately begin the hardening process.

One major issue in the wellbore design was the distance from the open hole section to the side of the block compared to the distance straight up to the top of the block. The distance from the open hole section to the edge was approximately 2 feet, while the distance to the top was 1 foot from the top of the open section. When pressurized, the fluid will take the quickest path to atmospheric pressure, which in this scenario is straight up. There were two main areas of concern with this problem. The first was the ability for the epoxy in the annulus to successfully prevent the fluid from channeling upward through the epoxy layer. The second concern is that even if the epoxy holds, the fluid could channel around the annulus through the block and out the top. This is not an issue for field acid jobs due to the overburden pressure of the rock and the thousands of feet to surface. The first idea was to place large weights on top of the block to increase the overburden pressure, however, the weight that was required to shift the greatest pressure gradient to the side of the block was unreasonably high. The second idea is the one that was used, and it was to place a layer of epoxy on the top of the block along with a steel plate in an attempt to

create a no flow boundary. The hope in this is that fluid cannot travel through the epoxy and the plate, which means the quickest path to atmospheric pressure would be outward. Because this idea was being applied to the top of the block, it made sense to additionally add a layer of epoxy and a steel plate to the bottom of the rock because it is possible that the pressure gradient is also greater in that direction than outward.

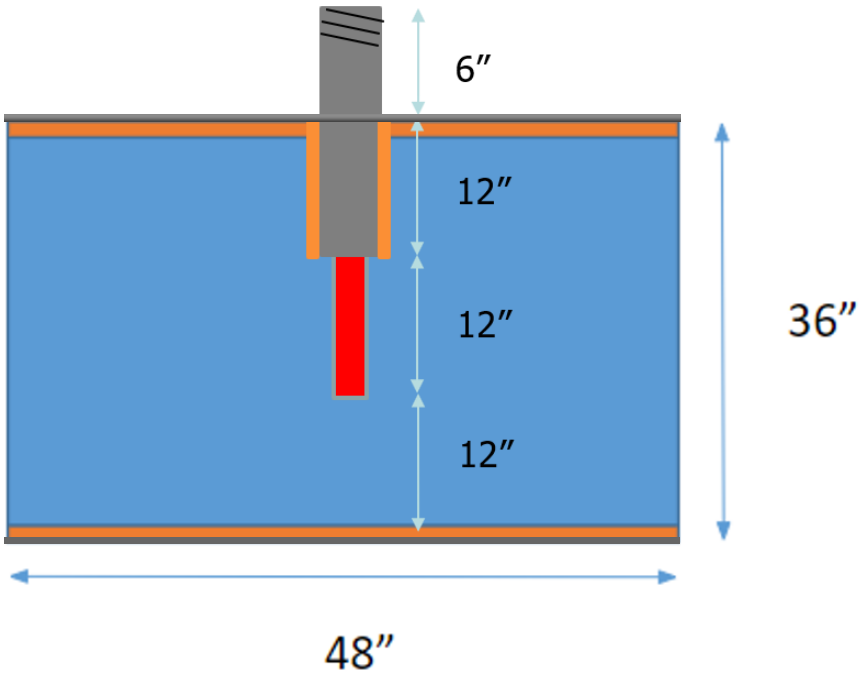

Figure 6. Wellbore mockup design

Once the wellbore plan was in place it came time to execute it. First, with the help of Kocurek Industries, the block was flipped upside down, and the epoxy layer was applied to the bottom of the block. Before it set, the steel plate was quickly placed on top of the epoxy and cinder blocks were placed on top of the plate to aid in the adhesion between the block, epoxy, and plate. The epoxy had a final cure time of 48 hours, so it rested until fully cured. Once cured, the block was flipped again using a large forklift to be oriented correctly. Similar to the epoxy

layer on bottom, the second epoxy layer was applied on the top of the block and the steel plate placed on top of the epoxy with cinder blocks.

Figure 7. Bottom steel plate and epoxy layer

It is important to note that the steel plate for the top of the block has a 2-inch hole cut in the middle for the wellbore. Once this epoxy layer had cured, the wellbore drilling commenced. First, the 2-inch diameter hole was drilled 1 foot into the block while flowing water to prevent overheating and to clear any cuttings as seen below.

Figure 8. Coring machine

There was not an easy way to get the core out of the block, so Kocurek used a hammer to lightly tap the core in the hopes that the bottom of the cored section would fracture and break free from the rest of the block. The core broke in half leaving two approximately 6-inch cores as seen in the following two figures. The top half was pulled out easily, but the bottom half was more difficult to remove. A corkscrew drill was used to latch on to the core to rip it out of the block.

Figure 9. Wellbore core after drilling

Figure 10. Broken core

For the epoxy to properly adhere, the area must be completely dry, so the block was left outside for 2-3 days to dry along with the use of a vacuum to suck out any additional water droplets left inside. Because the hole drilled was exactly 2 inches, the pipe had to be slightly smaller to fit in the block. The pipe chosen was 1 ⅞ inch and 18 inches long, and had a plastic cap on the bottom to prevent epoxy from entering the inside of the pipe and sealing the wellbore. Using the same epoxy as used for the top and bottom of the block, a very thick layer was pressed on all sides of the pipe. Quickly, the pipe was placed all the way into the block, and excess epoxy was forced out the annulus and rested on top of the block. Using a shorthanded shovel, the excess epoxy was pushed as close to the pipe as possible to help seal the area between the pipe and the hole cut in the plate.

Figure 11. Pipe coated with epoxy layer

In addition, a ruler was used to ensure the pipe was sticking 6 inches out of the block so that it could be confirmed the depth drilled was 1 foot. The epoxy was left for another 2-3 days to fully cure. Once cured, the open hole section was ready to be drilled. The block was carefully placed into the coring machine to avoid hitting the pipe already in place. The open hole section was now drilled, and again water was flowed to prevent overheating and brought up cuttings.

Figure 12. Coring machine in use for open hole

The core for this section was difficult to remove because the bottom is below 6 inches of pipe plus 2 feet of block. A long rod was used to try to fracture the bottom. This proved successful because after a vacuum was used to suck and lift the core out of the wellbore. The

core's length was measured, and it was only 11 inches long as seen in the figure below. This meant there was still an inch of core left inside the block. It was difficult to extract, but Kocurek was eventually able to use a corkscrew drill to grab the remainder of the core and pull it out of the wellbore.

Figure 13. Open hole core

After this was all completed, the block was transported to the experiment site so that a crane could lift it into the experiment tank. The block was supposed to be delivered on a pallet so straps could be used to safely lift the block into the tank. When delivered, the block was sitting on the back of a trailer without a pallet, so there was nothing underneath to safely attach straps.

The rigging crew decided it was best to place the straps around the side of the block to lift it momentarily to slide a pallet underneath that could then be safely used to lift the block into the tank. During the initial pick up, the straps did not squeeze the block hard enough, and lifted up on the block pulling a corner of the plate off the block entirely as seen below. The red circle is the corner where the lifting straps pulled the plate off the block.

Figure 14. Block as it was lifted onto pallet

This was catastrophic because the no flow boundary was now destroyed. The initial thought on site was to completely take the plate off the block and start over, but the project was behind schedule, so the decision was to do a quick patch job after the block was inside the tank.

While this was not the ideal result, the block was able to be lifted onto the pallet on the second attempt. The crane could now put straps underneath the block and lift it more safely.

Figure 15. Block and tank setup

The hand signal in the figure above was to tell the crane operator to slowly lower the block into its resting place. The crane then lowered further to remove the straps. After the block was inside the tank, then the tank lid had to be placed on top. The lid was far too heavy and big to be picked up, so once again the crane was used to place it on top of the tank. The lid had a few handles on the top, so the same lifting straps were used to pick it up. The only tricky part was the lid and tank had holes where bolts needed to be placed to secure the lid on top. One of the small

holes can be seen in the foreground of the above figure. It was difficult to maneuver the lid to get the holes to line up precisely with those of the tank, because the lid did not spin very easily. There were multiple people standing around the tank that quickly fastened the bolts on when the holes matched up. The following figure is a picture taken inside the tank after the bolts were securely fastened.

Figure 16. Block and tank setup with lid

The hole in the tank in the above figure is where the tubing would connect the pump to the block. Once the block was in the tank with the lid shut, it was time to complete the patch job of the plate that had been lifted. This consisted of using the same epoxy and a very thin

shorthanded shovel to push a new batch of epoxy as far back under the plate as possible and allow it to cure with cinder blocks on top. When attempting this, it was very difficult to push the epoxy far back without lifting the plate. It was difficult to know how far to push the epoxy to fully patch the plate, but not so far to lift sections of the plate that were still sealed with the epoxy.

Weeks after, a water flow test (described later in the paper) to check for leaks and ensure the system was operating correctly was performed, and the pressure reached values around 700 psi. During this test, water leaked out from multiple places between the block and the plate.

Figure 17. Water breakthrough

It started at the same corner that had been compromised when the block was lifted and the plate unexpectedly pulled off. Water was pumped for a short period of time after that, and 3 out of 4 edges of the block were leaking from between the epoxy and plate at the top of the block along with a leak coming from the annulus. It was quite obvious that the epoxy did not hold the pressure. At this point it was too late to redesign the plate, so another patch job was in order. For the best results possible, the entire plate was lifted off to completely redo the epoxy layer. When the plate was lifted, it could be seen that the epoxy did not adhere to the plate in most places, and the epoxy layer was so thin that water had broken through or pushed it out of the way all across the top of the block as seen in the figure below. For reference, the rough gray areas are where the epoxy actually did seal with the block. There was hardly a boundary to prevent fluid from flowing between the surfaces.

Figure 18. The plate (top) and the block (bottom) when pulled apart

A new epoxy called FlexSeal was used that had previously been tested on a linear core flood at a pressure of 1,000 psi and held without any faults. The initial test could not go to any higher pressures due to the pressure limitations of the piping that was in use during that test. This epoxy had a lower viscosity, similar to warm honey. A small containing wall was set around the block so that the epoxy could be poured on top of the block and spread out without it falling off the edges of the block.

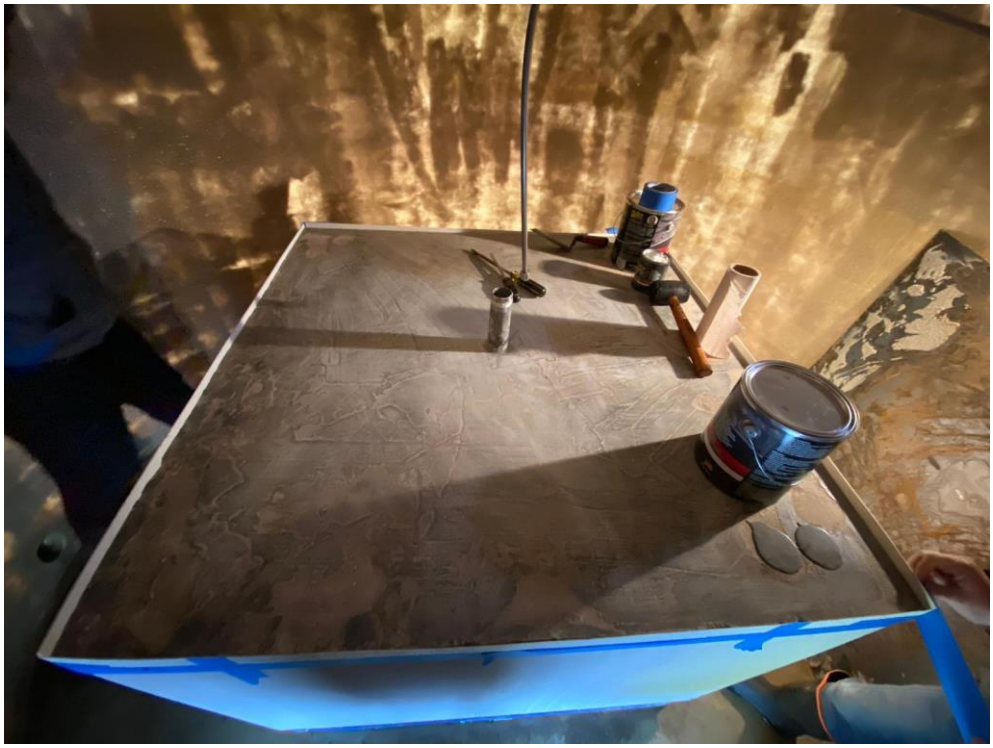

Figure 19. Preparation for FlexSeal epoxy

The containment wall shown above helped provide a thicker layer to prevent breakthrough. Similarly, to the previous epoxy, as soon as it was placed, the plate was set on top to adhere. The FlexSeal was poured from two large canisters along with a small batch that had

been used for the initial pressure test. The epoxy spread out fairly easily, but a small hand shovel was used to help spread to areas that had a smaller thickness.

Figure 20. Applied FlexSeal layer

The containment wall did a good job of allowing the epoxy to build up to a thicker layer, but some areas did not hold. In those cases, the epoxy ran down the side of the block, and a layer of tape had to be placed very quickly to prevent the epoxy from leaking more. It looked messy, but it appeared to have worked. The plate was quickly placed on top of the block to adhere to the epoxy. Directly after the plate was set, a FlexSeal spray can was used around the edges of the block between the plate and the containment wall. The idea of this was to form one additional layer of protection to force the fluid through the block and not between the block/plate boundary.

3.2 Scale Up and Pumping Conditions

The design parameters were based on the scale up model provided by Schwalbert (2019) found in the literature review. The core optimal pore volumes to breakthrough and interstitial velocity used for the scale up were 0.41 and 1.3 cm/min respectively. The calculations for the field scale up can be found in Appendix A. The results of those scale up calculations give the large-scale experimental condition values for the optimal pore volume to breakthrough of 0.059 and the optimal acid flux of 0.18 cm/min. Ideally, the pump would be adjusted throughout the experiment to stay at the optimum interstitial velocity. However, after conducting a few water tests, it was apparent that it would be very difficult to stay at the optimal acid flux throughout the experiment. The mass change used to calculate flow rate was not accurate in short periods of time needed to make those in-time adjustments. To recall, it is more efficient to pump above the optimal interstitial velocity and not below. Instead of trying to adjust the flow rate while pumping acid, it made more sense to keep the pump at the same rate and to keep the flux above the optimal for the duration of the experiment. The most practical solution to this was to set the pump at the rate in which the optimal acid flux would be reached right at the time of breakthrough as can be seen in calculations found in Appendix B. Theoretically, the pump rate for the interstitial velocity to reach its optimum value at breakthrough is 190 mL/min.

Figure 21. Dial on the pump used to control capacity

The pump used for this experiment has a dial that can control the capacity of the pump, which in turn controls the flow rate. Each tick shown above represents 1% capacity. With zero back pressure, the pump's maximum flow rate is 1 L/min. However, when pumping into the block, there was substantial back pressure affecting the flow rate produced from the corresponding capacity of the pump. Therefore, water injection tests were performed at various pump capacities with back pressure. During these experiments, a scale was placed under the water holding tank to measure the change in mass throughout the injection. The pump was placed at a specific capacity that was held constant. When the pump was first turned on, the

pressure response was near atmospheric for a few minutes while it filled up the tubing and wellbore before skyrocketing up to 500-800 psi depending on the flow rate as it was forced to flow through the block. After the pressure jump, the pressure leveled out and slowly oscillated within a 50-psi range. After the pressure leveled out, then mass measurements were taken over a 10-minute window to record the flow rate and pressure. This was done several times at various capacities to get a relationship between the capacity of the pump and flow rate as shown below:

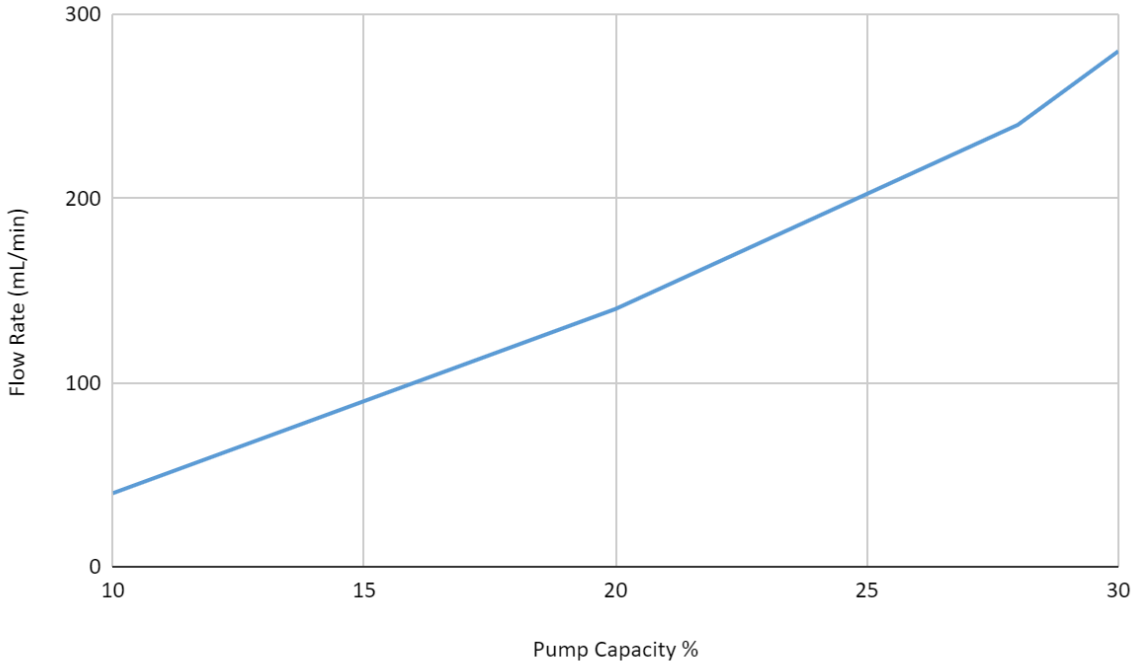

Figure 22. Relationship between pump capacity (%) and water flow rate (mL/min)

One important note, the tests for flow rate were done with water, not acid. 15% HCl is slightly denser than water with a specific gravity of 1.070 A simple calculation was used to find the water flow rate that would give the optimal acid flow rate of 190 mL/min:

$$q_{water} = q_{acid}\frac{\rho_{acid}}{\rho_{water}} = 190\ mL/min\frac{\frac{1.070g}{cm^3}}{\frac{1.000g}{cm^3}} = 203.3\ mL/min$$

In order to achieve that, the pump would need to be at approximately 26% capacity.

3.3 Experimental Setup

Texas A&M conducted another large block experiment at the University Services building, just off campus, a few years prior to this study. Some of the equipment used for that study were able to be salvaged. First was a small berm wall used to contain the site in case of spills. It measured about 1 foot tall and was made of cinder blocks that surrounded the test site. A black tarp was placed on top of the cinder blocks and pulled tight to prevent any leaks from leaving the containment area. The most important equipment salvaged was a large tank that measured 10 feet in diameter and 7 feet tall and was made out of carbon fiber material that would house the block. The block for this experiment would be able to fit inside the tank with 3 feet to spare on each side. During the experiment, the block sat in 4 feet of water, 1 foot above the top of the block. At the bottom of the tank, there were two outlet drains that connected to long hoses. The purpose for this was to have a contained place to flow the acid-water mixture after the experiment to dispose of the acid safely and in a controlled manner. When first arriving at the site, it had been 1-2 years since anyone had used the experiment tank. It had a few inches of water along with a lot of algae growth and small insects similar to a swamp. A sump pump was used to suck out the water, and then a mop was used to clean out the rest of the algae that had been growing in the tank. After that, the site was unaltered until the block was placed into the tank.

Figure 23. Experimental setup during construction

The figure above shows the actual experimental setup during construction. The experiment tank is the large gray cylindrical tank in the background. The water and acid inlet tanks can be seen in the foreground in white buckets. The water bucket is the larger of the two, and the acid was in the smaller bucket. Each bucket was taken from the lab where they were used for linear acidizing experiments. To the left of the buckets in blue is the pump with the inlets underneath it and the outlet near the tall grey cylinder on the top. Just behind the acid inlet tank is the waste tank, and to the right of that is the pressure transducer. The figure below shows the setup in a flow diagram.

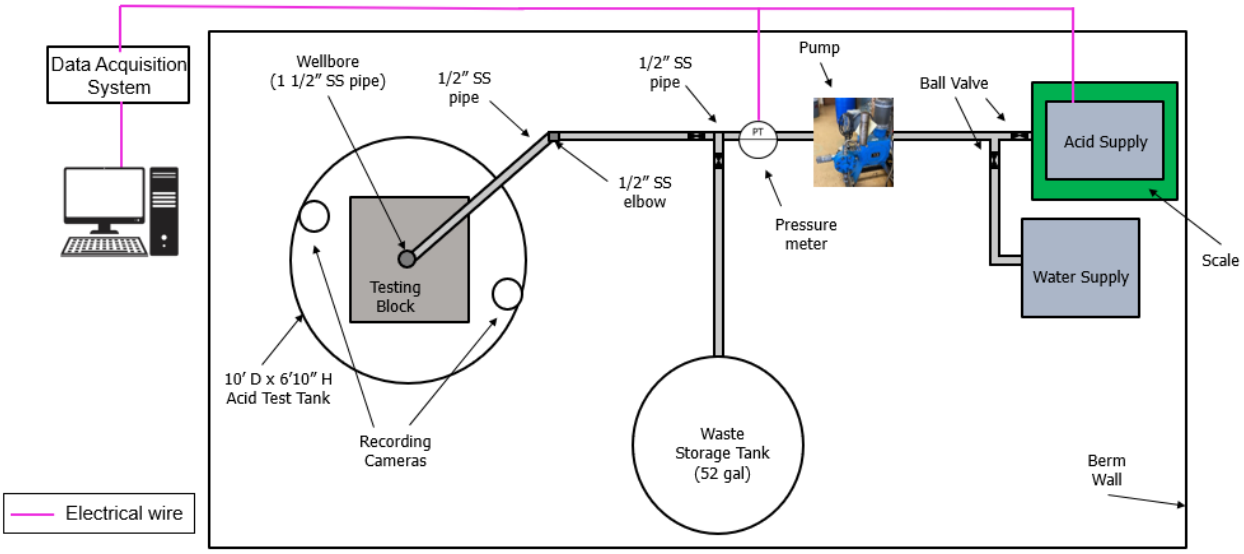

Figure 24. Experimental setup as a flow diagram

The first piece of equipment in the flow diagram was the two inlet tanks shown on the right side. The acid tank was sitting on top of a scale that would be used to measure the mass change over time to calculate the volumetric flow rate. Both of the tanks fed into the pump with 2 gate valves. The pump used in this experiment was a diaphragm pump built with corrosion resistant material that can pump up to 1 L/min assuming no back pressure. A waste storage tank was used to establish flow and to clear the lines of any acid after the experiment.

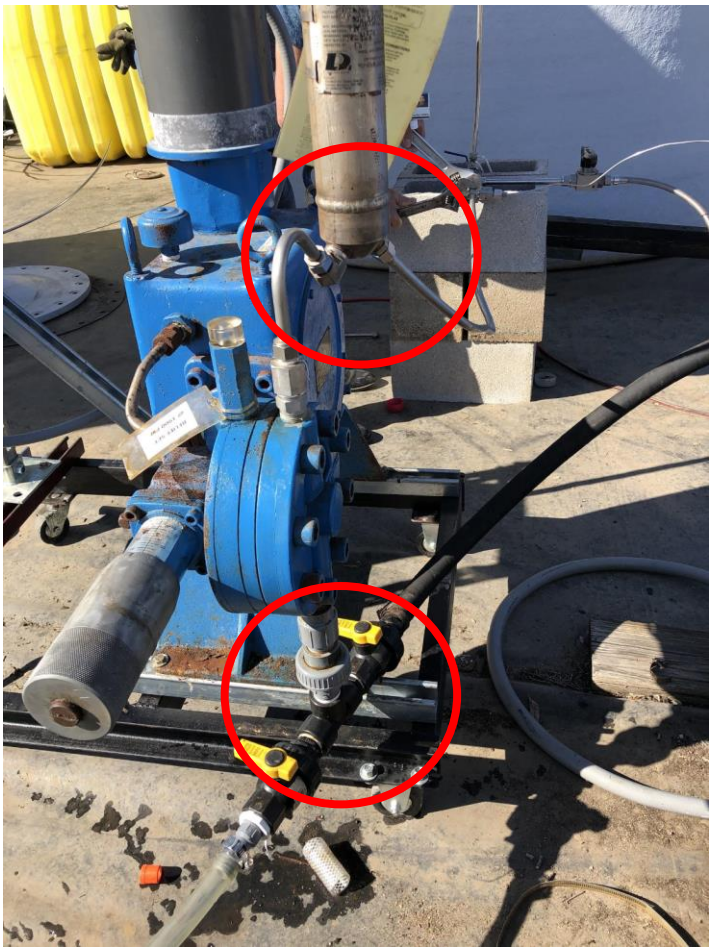

Figure 25. Pump at site with inlet (bottom) and outlet (top)

The pump outlet size was ½ inch, and the wellbore inlet was 1 and ½ inch, so fittings were required to make the connection. ½ inch stainless steel tubing was cheaper than 1 and ½ inch tubing, so the fittings were placed directly above the wellbore. This allowed the entire system to use the cheaper tubing until reaching a few inches above the wellbore. Both the tubing and fittings were rated to 3,000 psi to hold back any pressures that might be seen during the experiment. The ½ inch tubing leaving the pump led first to a T where one end led towards the block and the other went to a pressure transducer. The pressure transducer was powered using a computer combined with an Arduino board. The Arduino board captured the voltages transmitted

from the pressure transducer and converted them into pressure values that could be read on the computer either in a text file or a graph.

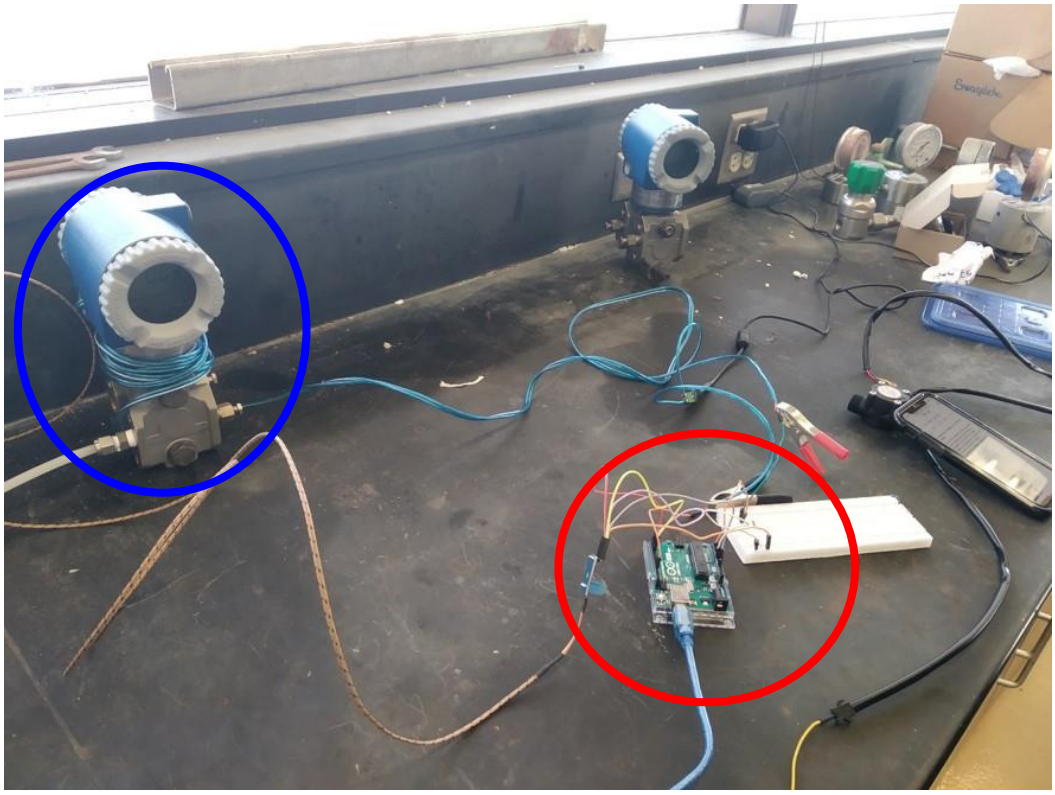

Figure 26. Pressure transducer (blue) and Arduino board (red)

The red circle in the figure above is the Arduino board as it was being set up. After it was working, it was placed in a plastic box with outlets for protection. The blue circle is a pressure transducer used to measure the pressure and feed the information to the Arduino board.

It was critical to know the pressure in the tubing at all times for safety reasons. After passing the pressure transducer line, there was a T. The first direction went directly to the block with a needle valve to control flow, and the second direction led to the waste tank, which also had a needle valve. The line to the waste tank was used to establish flow at the beginning of the

experiment along with the purpose to clean out the lines at the conclusion of the experiment. The last piece of equipment used for the experiment were a pair of Arlo cameras. They were magnetically mounted using metal connections adhered to the fiberglass tank near the top of the tank. Each one was connected to a base station by Wi-Fi, and the base station was connected via ethernet cable to the University Services building. The base station then recorded the video that each camera output and displayed it on the Arlo website. A computer used the "Screen Share" and "Record" abilities of zoom to capture the live video and save it as a backup file to the one saved on the Arlo website.

Figure 27. Arlo camera mounted in tank

The cameras were used in this experiment first and foremost for safety purposes. If there was a leak, or acid was spraying in the tank, then it would be visible from the cameras and the

experiment could be shut down safely. The cameras were also used to visualize breakthrough. When the acid reacts with the rock, carbon dioxide is formed. When the acid breaks through the end of the block, the carbon dioxide will be easily seen bubbling up through the water. That signals to the researchers that it is time to switch the pump back to water to push any remaining acid through the system.

3.4 Experimental Procedure

There are two different sets of procedures that were used for this study. The first procedure was used for water tests. The water tests determined the flow rates at different pump capacities with back pressure, established that there were no leaks in the system, tested all recording equipment, and saturated the block close to the wellbore. First, the waste line was opened and the valve going to the block was closed. After this, the pump was turned on to establish flow at the specific capacity. Once there was flow into the waste tank, then the valve to the block was opened, and the valve to the waste tank was shut. The pressure increased very rapidly as the water was being forced into the pores of the rock. The fittings and tubing were checked for leaks along with the pressure transmitter output. After checking for leaks and the pressure stabilized after a few minutes, the flow rate could be calculated based on the mass change per time. This was done for various pump capacities to find the correlation between capacity and flow rate along with the given pressure at that flow rate. The results of this procedure are found in section 3.2. Once this was completed, then the pump was shut off and there was a wait period to allow the pressure to decrease as the remaining water slowly seeped into the block. Once the pressure dropped below 50 psi, the waste line valve was opened slowly to release remaining pressure and to clear the lines of water.

The acid test procedure had a lot of similarities to the water test with a few key additions. The first addition was the PPE. When dealing with acid, it was essential to have the right gear. Anyone near the apparatus needed a fitted gas mask to prevent inhaling any fumes. They also needed a full acid resistant coat that covered all skin. Gloves were worn to protect hands from any chemical spills. Jeans were worn underneath the acid resistant coat with rubber boots to further deter any acid spills from injuring a person. In addition, there were washing stations and acid spill kits at a designated area.

Figure 28. Proper PPE while adding acid to inlet tank

For the procedure itself, first, the cameras needed to be set up inside the tank and connected to the computer to ensure that they were working properly. After this, the long process of filling the tank with water began. Based on the flow rate of the garden hose coming out of the

building, it took approximately 6 hours to completely fill up the tank to 1 foot above the level of the block. While this was occurring, the pressure transmitter and scale were turned on. The water level could be seen by checking the cameras on the computer. Once it reached the appropriate level, then the hose was shut off. Then, the experiment began similarly to the water test. With the valve to the waste tank open, the pump was turned on to establish flow. When flow was established, then the valve to the block was opened, and the valve to the waste tank was shut. The pressure increased rapidly but stabilized as the water forcefully flowed into the block. This was a critical time to check for leaks or any other apparatus issues right before the switch to acid. After the pressure stabilized, then the inlet to the pump was switched from the water tank to the acid tank. The pressure had a sharp decrease as the acid began to dissolve the rock and then steadied out once again. The camera feed was monitored on the computer to see exactly when the bubbling of the carbon dioxide could be seen. At the same time, the pressure transmitter was monitored to look for a large decrease to atmospheric pressure as breakthrough occurs. Once breakthrough occurred, which was noticed first by the pressure monitoring, and then shortly after using the visual aid from the cameras, then the pump inlet was switched back to water to clear the lines of any remaining acid into the block for safety purposes. After enough time had passed and the pressure transmitter read atmospheric pressure, then the valve to the waste tank was opened to continue to clear out the lines and check for pH. When pH reached 6-7, then the pump was shut off. The fluid in the experiment tank containing water and acid was then released in a controlled manner into a waste tank to check pH. According to Texas A&M guidelines, if the pH was above a 4.5, then it could be dumped into the surrounding grass area. If the pH was below a 4.5, then all the fluid would need to be treated as hazardous waste through the university. In this case, the pH was between 6 and 7 by using pH strips. While this seems high after pumping acid,

the majority of it had reacted. In addition, it was calculated prior to the experiment that if all the acid in the inlet tank had somehow made its way into the experimental tank and none of it reacted, the pH was around 4.3. This gave great confidence that the post experiment pH would be in the safe zone and could be dumped.

3.5 Modeling with Solidworks and Ansys

In addition to the experiment, it was also desirable to generate velocity streamlines for a water injection assuming homogeneity of the entire block. Generating streamlines for the entire block is very messy and difficult to view in 3D. Because of the assumed homogeneity, the streamlines should be symmetrical. The geometry for the simulation will then be one quarter of the block in the top half, an eighth of the overall volume. The streamlines could be used in conjunction with CT scans taken of the block after the acidizing experiment to compare the paths taken by each of the fluids.

The simulation was first attempted by programming in Eclipse and visualizing the streamlines in Petrel. While Petrel was able to show streamlines, it did not have the capability to show how the velocity changed throughout the block.

Ansys Fluent is known for modeling flow and is relatively easy to learn. Fluent runs through a main hub known as Ansys Workbench. Workbench combines several programs through a work tree that initialize geometry, create mesh used for flow calculations, compute the calculations, and visualize the solution.

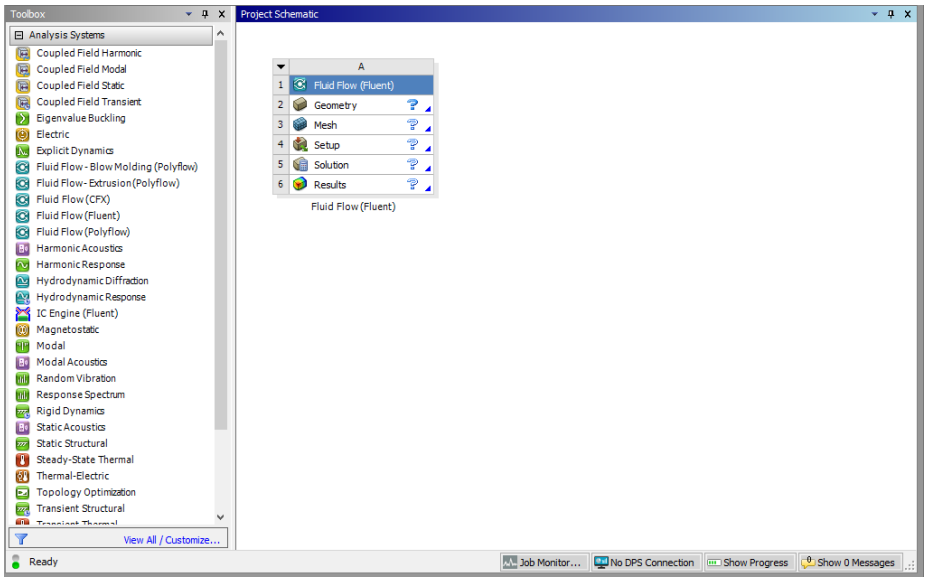

Figure 29. Workbench setup

Each program starts with a question mark until it is completed. The program shows a red X if there is an error either with that section, or if it is unable to progress to the next section based on selections.

The geometry can either be completed through the provided Ansys program or can be imported from other programs. Solidworks was chosen for the geometry because of its simplicity and there are a large number of tutorials available for the software to create any type of geometry. As mentioned earlier, the geometry for the simulation is only a quadrant of the top half of the block. The easiest way to do this in Solidworks is to first create a square that measures 24 inches by 24 inches. The “Extrude Boss/Base” function can then be used to give it a height of 18 inches. The open hole section is created by using the “Simple Hole” function. The location will be on the bottom vertex with a radius of 0.5 inches and extends 6 inches upward.

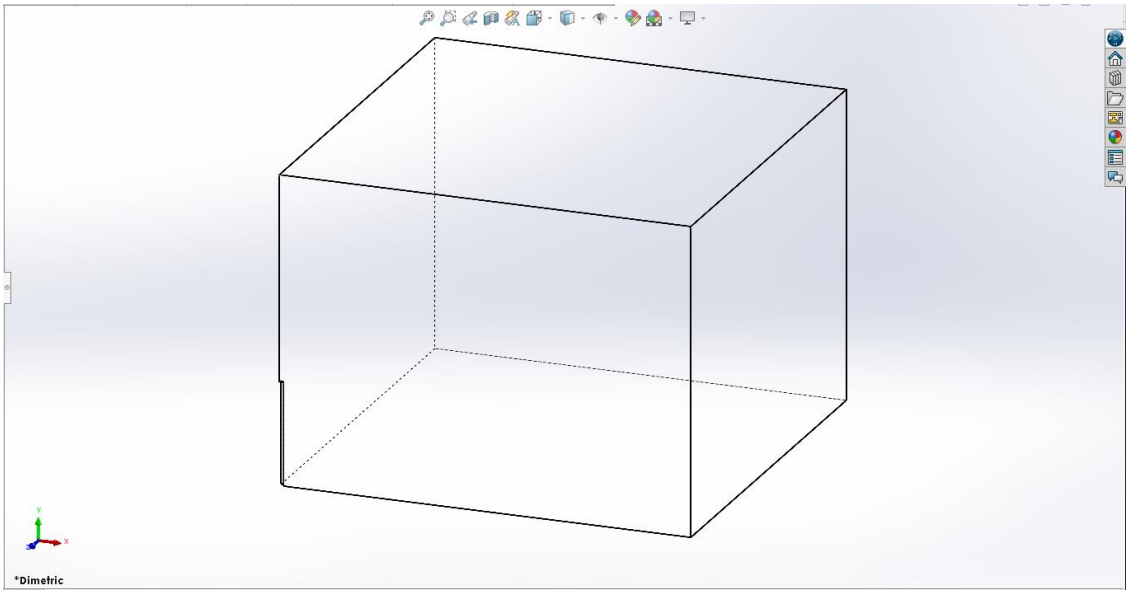

Figure 30. Solidworks geometry

Now that the geometry is complete, the mesh needs to be created for the block. The mesh divides the block into smaller pieces for flow calculations similar to creating a grid in a reservoir simulator. The near wellbore area is specified to have additional grid blocks because that is where the most diverse flow paths will be located. In addition to meshing, the walls are also named so that boundary conditions can be initialized in Fluent.

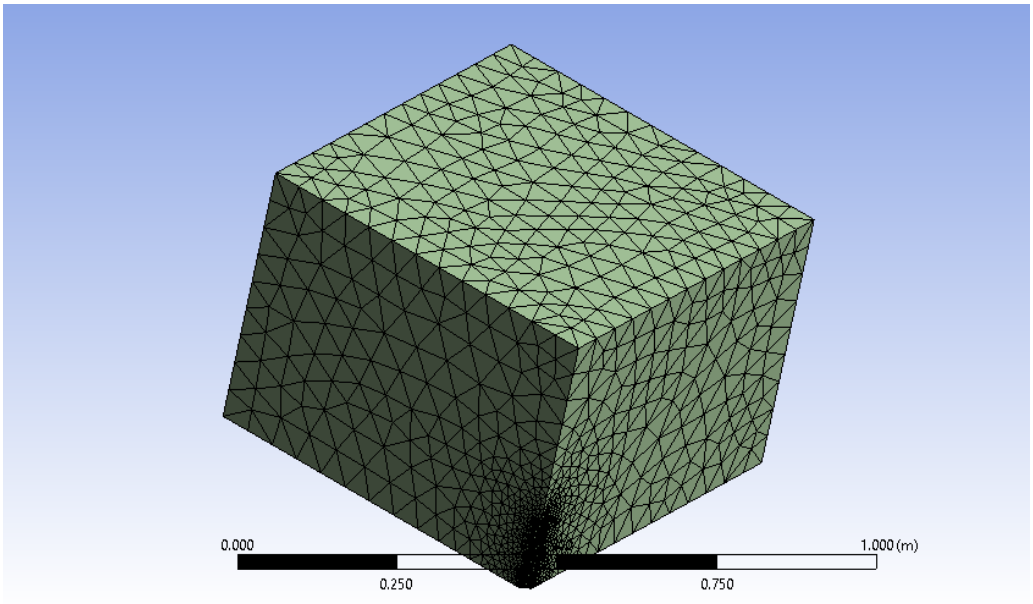

Figure 31. Mesh grid

From the view in Figure 31, the walls are labeled as “Front Left”, “Front Right”, “Back Left”, “Back Right”, “Top”, and “Bottom”.

The meshing will automatically import when Fluent is opened. The first step in the setup is to change the fluid from air to liquid water. Under the “Cell Zone Conditions”, the entire block is selected, and the porosity/permeability values can be input. After that, the boundary conditions will be specified using the labeling from the previous paragraph. The “Front Left”, “Front Right”, “Top”, and “Bottom” will all be considered “Wall”, the Fluent term for no-flow boundary. The top of the block has that category because of the plate, the others are all classified as no-flow boundaries for the symmetry of the block. The open hole section is labelled as “Inlet”, and the “Back Left” and “Back Right” are “Outlet”.

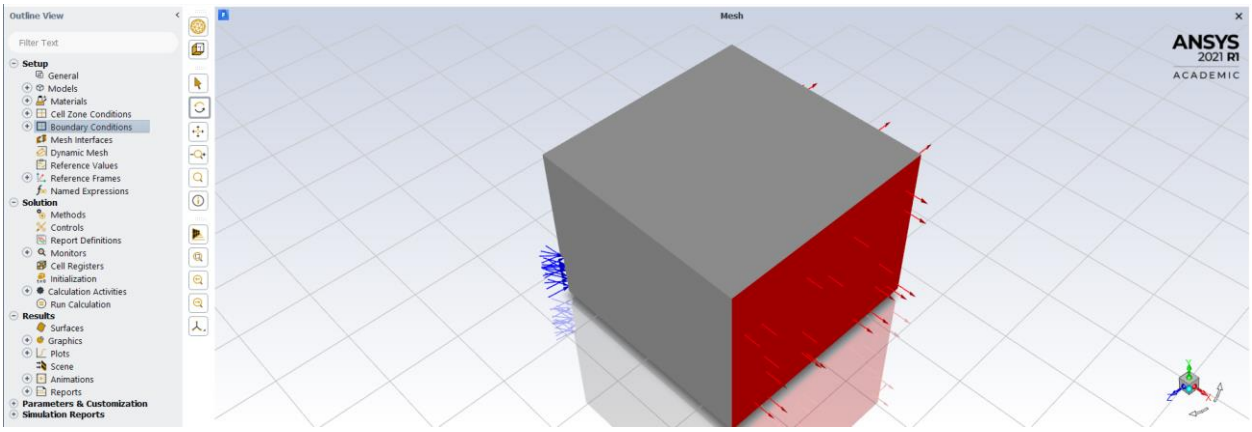

Figure 32. Fluent setup

After selecting the boundary conditions, they are visualized as shown in Figure 32. The inlet is shown with blue arrows, outlets are shown with red arrows, and the walls are shown as grey. All other parameters are kept at the pre-defined values. The program can now be initialized and calculated.

4. RESULTS

The day of the experiment was mostly successful, with only a minor delay due to the building's water being shut off part way through filling the tank to fix issues inside the building. It lasted approximately 3 hours, but because the tank started filling up near 5 AM, the experiment was still able to be run that day. The video feed of the cameras occasionally had issues connecting to the computer, but there was always at least one camera working to view the inside of the tank. Below are photos from the two cameras directly before and after the breakthrough occurred. The breakthrough can be seen in the circles that show the carbon dioxide bubbling up through the water in the tank forming ripples.

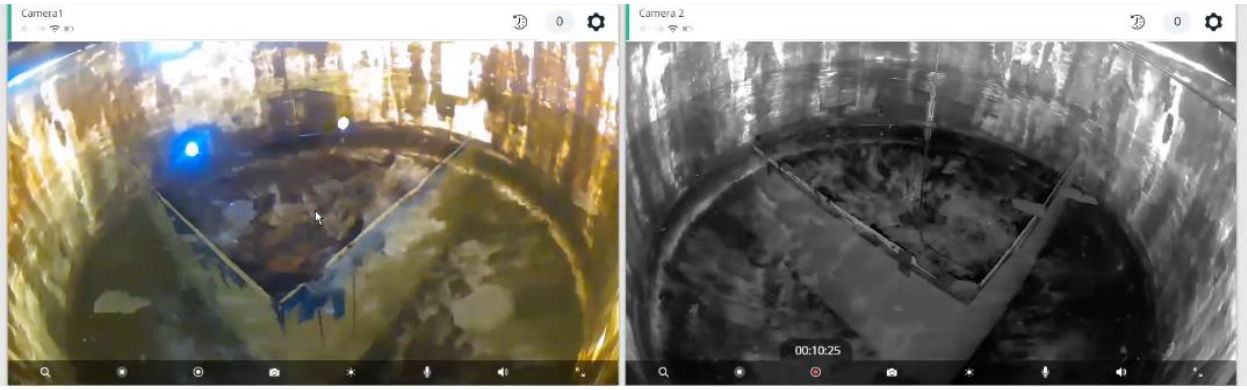

Figure 33. Arlo cameras before breakthrough

Figure 34. Camera 1 after breakthrough

Figure 35. Camera 2 after breakthrough

After the experiment concluded, and the pH was close to neutral, the water was safely released into the nearby field. A few days after the experiment, the block was lifted out of the tank using a large crane to be taken to Kocurek Industries to be cut as shown below.

Figure 36. Block removed from tank after acidizing

When the block was placed on the trailer, it was quite visible where the rock was acidized by a large stain. However, upon inspection of the video, this was not actually the corner where the bubbling occurred. The dissolution shown in the following figure corresponds to the front corner seen in Figure 34.

Figure 37. Acid stain on block

There was tape covering this section of the block, so it appears that the acid channeled down from the top of the block near the epoxy-plate boundary and got caught in that section between the rock and the tape. When the block was sitting on the trailer, the tape was removed, and acid poured out of that spot as though it were trapped under the tape. The pool of acid would explain the large gouge left in the rock. The section where the bubbling occurred and the section with the large acid stain were CT scanned, and no wormholes were found in either section. This suggests that the acid travelled through the annulus and then across the epoxy-plate boundary until it finally broke through at the edge. This is shown in the following figure. The corner where bubbling occurred is the same corner where water broke through during the water injection tests. There had been only a single layer of sprayed epoxy that resealed the edge of the block.

Figure 38. Wellbore CT scan

The figure above is the CT scan of the wellbore section that includes the pipe. The porous space is represented in white. It is especially clear near the top of this picture that the acid channeled upward to reach the block's surface. The bulk volume dissolved in this scan was 79.79 cm^3. Based on the reaction of HCl with Calcite, 874 mL of acid was required to dissolve this volume.

After the experiment was finished, core samples were taken from the block to measure the porosity, permeability, and optimal values for interstitial velocity and pore volumes to breakthrough. The porosity value was found to be 9.1%, and the permeability was 1 md.

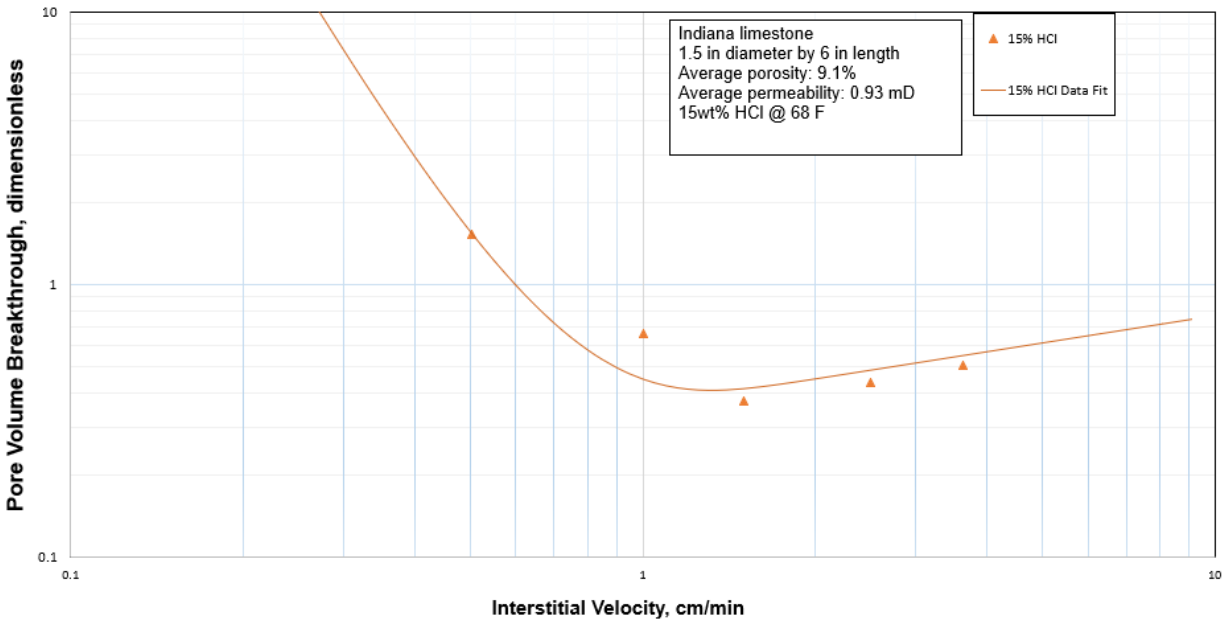

Figure 39. Optimal values found from large block

The cores were acidized, and the optimal interstitial velocity was 1.3 cm/min and the optimal pore volume to breakthrough was 0.41. Using the Schwalbert (2019) method, the values were scaled up to give the large block optimal values for interstitial velocity and pore volumes to breakthrough as 0.18 cm/min and 0.059 respectively.

4.1 Pressure and Flow Rate Data

The pressure data was recorded on the computer through the Arduino board, and measurements were taken every second. The mass data from the scale could not be uploaded to a computer automatically, so the mass data was recorded using a video camera that was aimed at the scale. Manual measurements were taken every 5 seconds. Flow rate was then calculated based on the change in mass every 5 seconds. The chart below shows the pressure data along with the mass of the acid tank. The amount of acid pumped prior to breakthrough was 2.2 L

assuming an acid density of 1070 kg/m^3. When subtracting out the amount of acid still in the lines, only 0.36 L were pumped into the block. There was additional acid that was pumped after breakthrough was achieved because the team waited until visual confirmation of bubbling from the cameras, and the cameras had a time delay of half a minute.

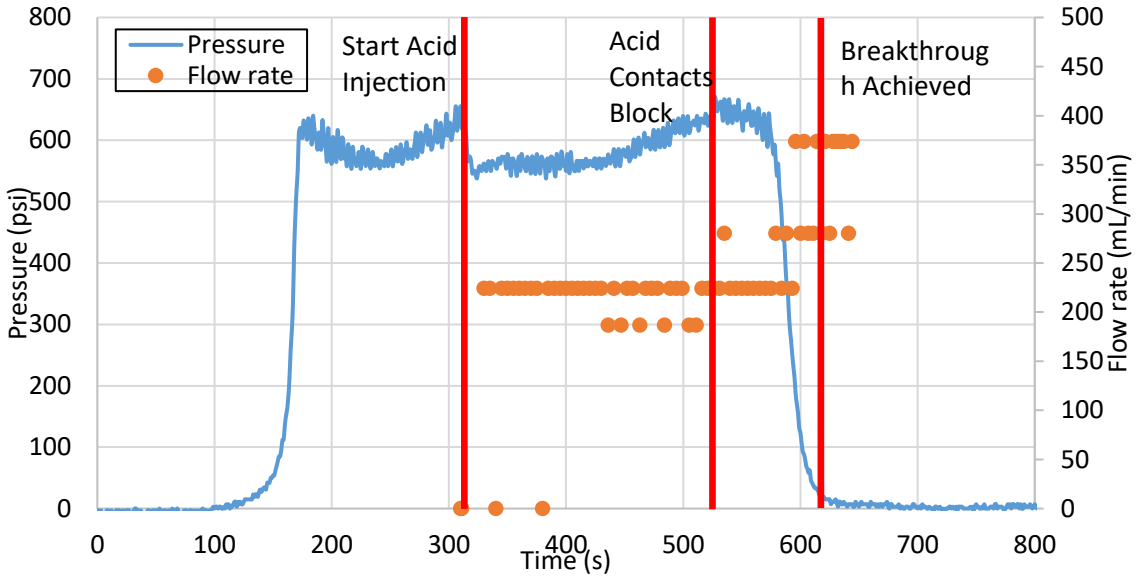

Figure 40. Pressure and flow rate data

The initial spike in pressure is when the flow switched from being pumped into the waste tank to the block which began at 90 seconds. Similar to the water tests, the pressure oscillated within 100 psi (570 to 650 in this case). The first vertical red line indicates the switch from water to acid at 310 seconds. This can be seen by the sharp drop in both the pressure and tank mass. The mass dropped more initially to fill the lines between the tank and the pump as expected. It took almost 4 minutes for the acid to reach the block as it travelled through the lines. The second red line indicating pressure increase seen at 527 seconds is when the acid contacted the rock. The pressure then decreased as acid dissolved the rock until breakthrough. The flow rate stayed mostly constant during injection at 225 mL/min with the exception of a few dips to 190 mL/min. The small drops were most likely due to the scale's lack of precision. It read to the second

decimal place, but more accurate scales were out of the price range. The large pressure drop near the 580 second mark is when the acid reached the edge of the block. Breakthrough was observed visually through the cameras at the second vertical red line of 620 seconds. Acid was pumped for a short time while the team confirmed the visual breakthrough before switching the pump back to water and shutting the valves from the acid inlet tank. It can be seen from the time difference between the red lines that the time of acid pumped was 5 minutes and 10 seconds, and the estimated time to breakthrough based on the pressure response is 1 minute and 33 seconds.

4.2 Comparison of Experimental Data with Calculations

There were some discrepancies between the theoretical time to breakthrough and the actual time to breakthrough. As mentioned above, the actual breakthrough time was 1 minute and 33 seconds.

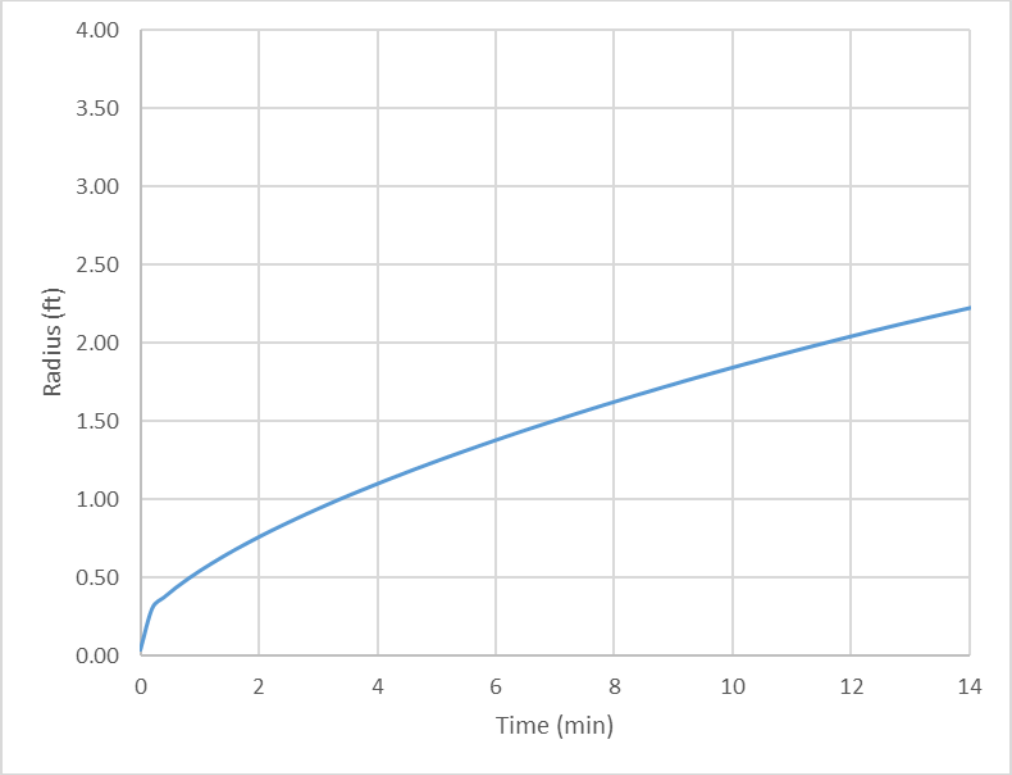

Figure 41. Theoretical wormhole propagation (Appendix B)

The chart shows that the time to breakthrough should have been 11 minutes and 30 seconds using the calculations from Appendix B. The volume pumped at breakthrough was 2.2 L in the theoretical case found in Appendix B compared to the 0.36 L that were actually pumped during the experiment to reach breakthrough. In terms of pore volumes to breakthrough, the theoretical value was 0.059, and the experimental result is shown in the calculation below, where 4.32 ft^3 is the pore volume of the block,

$$PV_{bt} = 0.36\ L \frac{1\ ft^3}{28.3\ L} \frac{1\ PV}{4.32\ ft^3} = 0.003 \tag{20}$$

4.3 History Match with the Schwalbert (2019) Model

A history match with the Schwalbert (2019) method was done to determine the flow rate required to get a breakthrough time of just over 1 and ½ minutes. Assuming the same scale up values for the calculation and using the optimal values found from the large block, the acid would have to travel at 1.9 L/min, a value that is not feasible for the pump used in the experiment even with no back pressure. The required volume of acid to reach breakthrough at this high flow rate is 2.8 L. This history match proves that the acid did not travel through the block, and instead travelled through the annulus and then along the epoxy-plate boundary until reaching the edge of the plate. Channeling around the annulus and across the plate is the only way the acid would be able to achieve breakthrough in such a short period of time.

4.4 Ansys Fluent Simulation

The Ansys Fluent simulation shows that the velocity in the near wellbore area is extremely large in comparison to the velocity exiting the block. The velocities in the plot are shown on a logarithmic scale in cm/s.

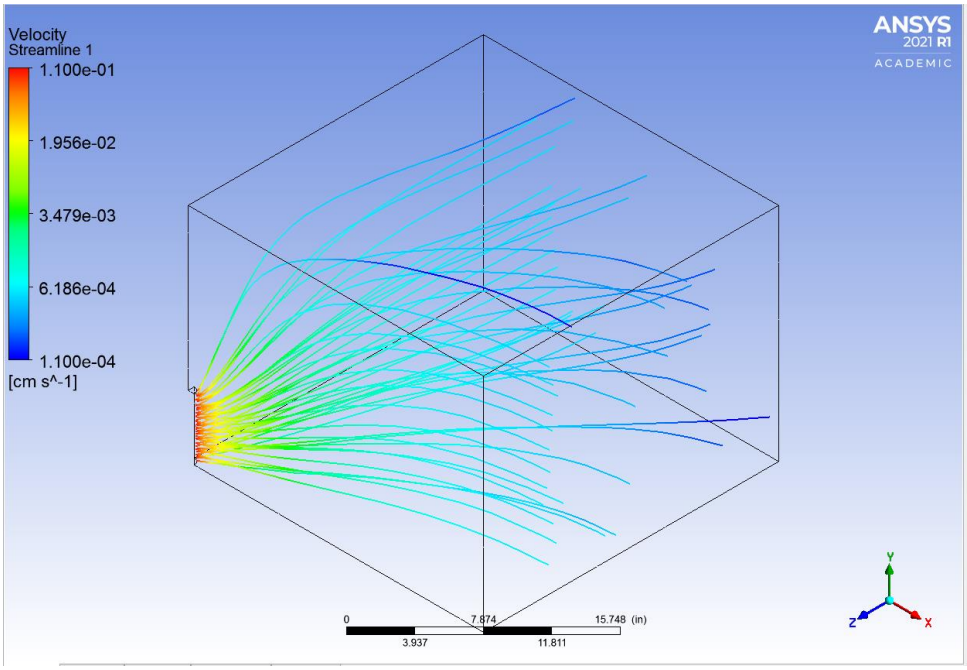

Figure 42. Generated streamlines shown in a 3D model

The velocity exiting the wellbore is 0.11 cm/s, and the velocity exiting the block is approximately 6.0E-4 cm/s for the majority of the streamlines, but goes as low as 1.1E-4 cm/s.

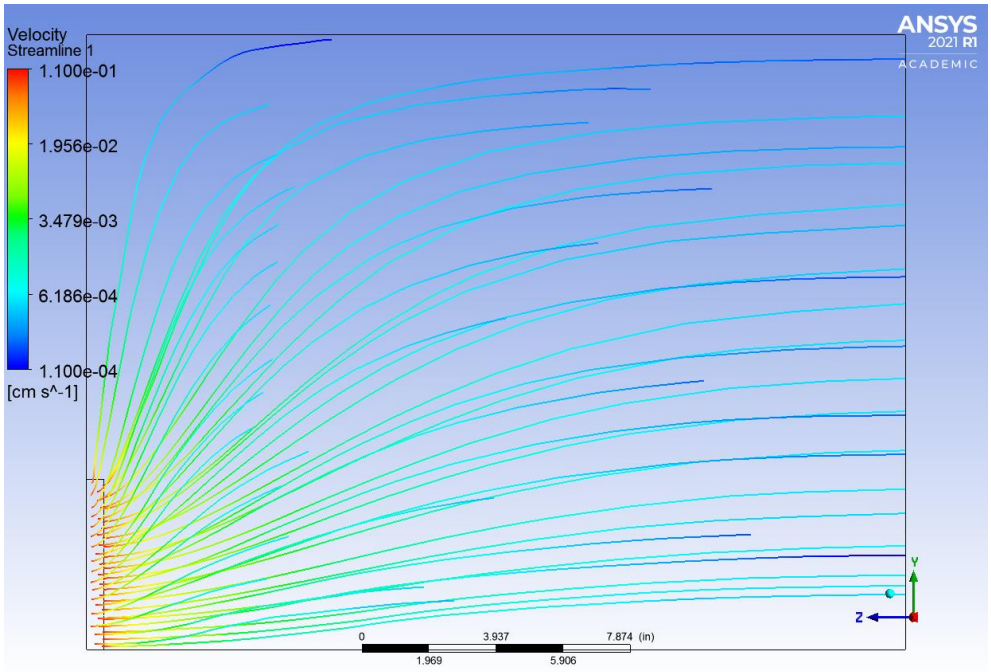

Figure 43. Generated streamlines side view

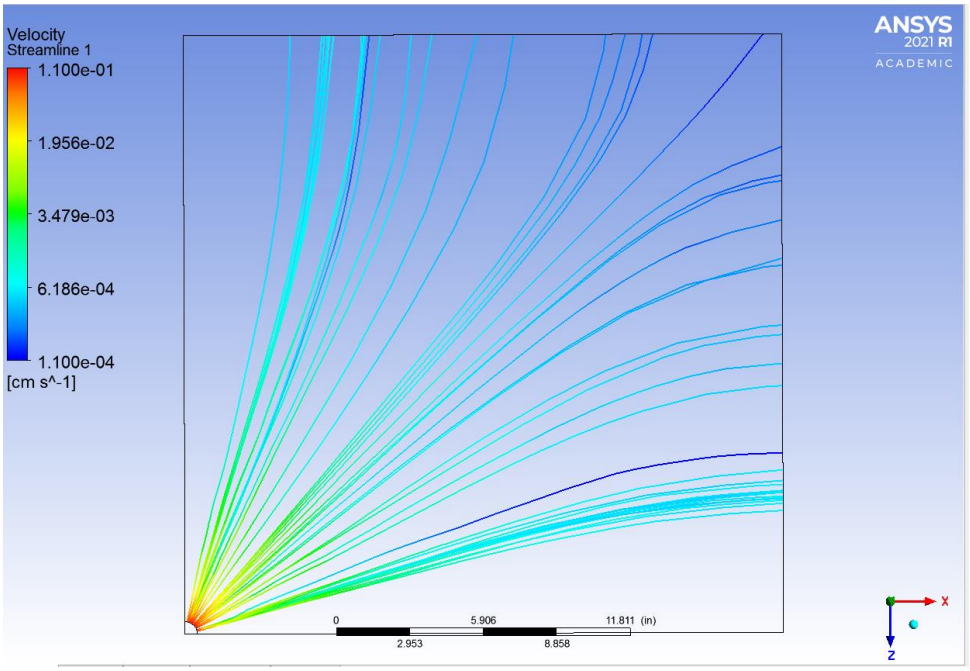

Figure 44. Generated streamlines top view

On the top view, there is a streamline near the lower section that is blue for almost the entire distance to the edge of the block. At first glance, this is worrisome, but when looking from a different view it can be seen that this particular streamline goes directly up and is near the top boundary causing the velocity to be so low.

When looking at the streamline velocity profiles, it is easily seen that the longer the pathway from the inlet to the exit position on the block, the more the velocities decrease. This means the shortest distance to the edge of the block results in the highest exit velocity. This can be used to predict the location of breakthrough on future experiments. Breakthrough will occur at the shortest distance from the inlet to the boundary of the block. It appears through this simulation that the breakthrough will occur at one of the four block facies at the same height as

the inlet with small discrepancies due to heterogeneity and open hole design. The last place for acid to breakthrough would be on any of the edges near the top or bottom of the block.

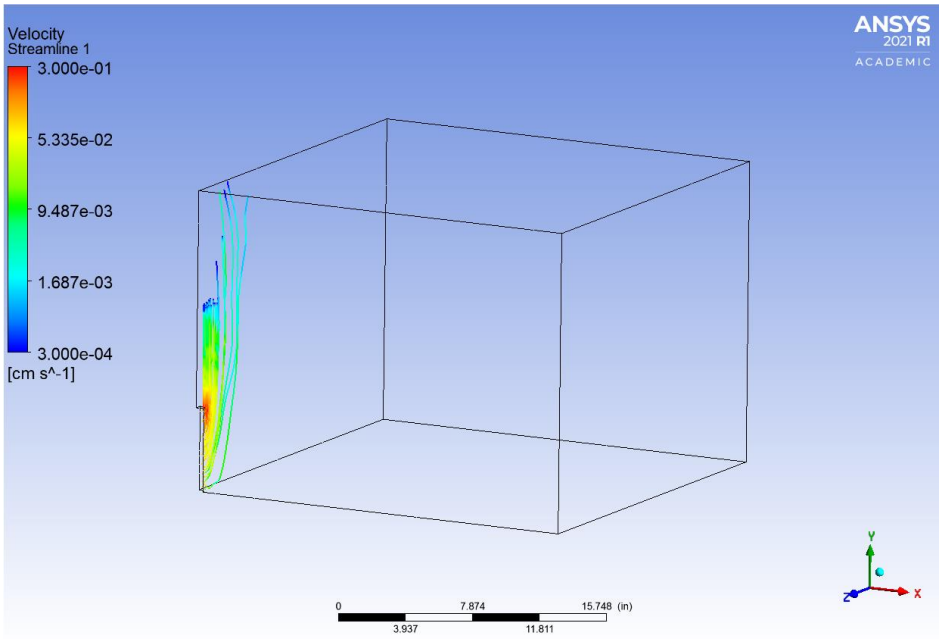

Figure 45. Generated streamline for acid channeling upward

The figure above shows the likely path that the acid travelled in the actual experiment. This was completed by changing the boundary conditions to allow the flow to exit the top of the block along with the vertical permeability being increased to 100 times the horizontal permeability.

5. CONCLUSIONS AND FUTURE WORK

The results seen were quite different from the calculations done prior to the experiment. All the data leads to one large conclusion which is that the acid did not travel through the block and instead travelled up the annulus and then across the top of the block before breaking through at the corner. It is important to note that the corner where the bubbling occurred was the same corner where water broke through during the water tests weeks prior to the acidizing experiment. The conclusion from this is that a channel had already been formed, and the only preventative measure to stop the seal from breaking was a thin layer of spray epoxy. The flow rate seen from the experiment was very close to the desired flow rate calculated, however, the remainder of the results did not relate to the theoretical values. The time to breakthrough was not close to the calculated value as it was off by over 10 minutes. The final piece of evidence that the acid did not travel through the block is the pore volumes to breakthrough. The scaled optimal value was 0.059, and the actual pore volume to breakthrough was 0.003.

There is a lot of future work that can be done to add on to this study. The HCl test will be redone, along with experiments using synthetic acids. Most of these acid systems have optimal interstitial velocities below that of HCl, so experimental conditions should be changed. They should be run at their optimal values to get the best comparison of the acid systems when performing at their peak performance. Another study could be to run experiments at various interstitial velocities to create efficiency curves in large block experiments for each acid type. This has not been done before, and would provide a lot of valuable information on the way that radial floods are being scaled from linear core floods. One obstacle in this would be to obtain enough large blocks to be able to do the study economically and in a reasonable time frame.

It could also be very beneficial to try to replicate reservoir conditions as closely as possible. A similar apparatus to the McDuff (2010) experiment could be used to get reservoir overburden pressures. It would be difficult to achieve and possibly very expensive, but then the issue of the fluid flowing directly upward/downward due to a shorter distance to atmospheric pressure would be solved giving more accurate results. Another consideration to get the experiment closer to reservoir conditions would be to heat either the water reservoir containing the block or the acid prior to injection. Changing the water in the tank may not affect results that much because the contact the water bath has with the tubing is brief. Heating the acid has been shown in previous studies to change its performance quite a lot. Both options are very simple to achieve. To heat the water in the tank, a natural gas heater can be used in conjunction with a pump to create a closed circuit slowly heating the water up to reservoir temperature. The tank at the experimental site has a temperature limit of 120 F, so for this study to be useful, a different tank would need to be used. There have been many studies done recently at Texas A&M in acidizing experiments where the acid was heated up to 200 F, and should be simple to do. Tubing coils containing the acid will be placed in a heated water bath along with adding electric heating tape to the tubing after the coils to reduce heat loss from the water bath to the block.

REFERENCES

Buijse, M. A., & Glasbergen, G. (2005, January 1). A Semi-Empirical Model to Calculate Wormhole Growth in Carbonate Acidizing. Society of Petroleum Engineers. doi:10.2118/96892-MS.

Burton, R. C., Nozaki, M., Zwarich, N. R., & Furui, K. (2018, September 17). Improved Understanding of Acid Wormholing in Carbonate Reservoirs Through Laboratory Experiments and Field Measurements. Society of Petroleum Engineers. doi:10.2118/191625-MS.

Economides, M. J., Hill, A. D., Ehlig-Economides, C. E.: "Petroleum Production Systems". Prentice Hall, Upper Saddle River, NJ, 1994.

Furui, K., Burton, R. C., Burkhead, D. W., Abdelmalek, N. A., Hill, A. D., Zhu, D., & Nozaki, M. (2010, January 1). A Comprehensive Model of High-Rate Matrix Acid Stimulation for Long Horizontal Wells in Carbonate Reservoirs. Society of Petroleum Engineers. doi:10.2118/134265-MS.

Glasbergen, G., Kalia, N., and Talbot, M., "The Optimum Injection Rate for Wormhole Propagation: Myth or Reality?", SPE Paper 121464, presented at the SPE European Formation Damage Conference, Scheveningen, The Netherlands, May 27-29, 2009.

Hoefner, M.L., and Fogler, H.S., "Fluid Velocity and Reaction-Rate Effects during Carbonate Acidizing: Application of Network Model," SPEPE, 56-62 (February 1989).

Huang, T., Hill, A.D., and Schechter, R.S., "Reaction Rate and Fluid Loss: The Keys to Wormhole Initiation and Propagation in Carbonate Acidizing," *SPE Journal,* **5**(3), 287–292 (September 2000).

Izgec, O., Keys, R., Zhu, D., Hill, A.D., "An Integrated Theoretical and Experimental Study on the Effects of Multiscale Heterogeneities in Matrix Acidizing of Carbonates," SPE Paper 115143, presented at the SPE Annual Technical Conference and Exhibition, Denver, CO, September 21–24, 2008.

McDuff, D., Jackson, S., Shuchart, C., & Postl, D. (2010, October 1). Understanding Wormholes in Carbonates: Unprecedented Experimental Scale and 3D Visualization. Society of Petroleum Engineers. doi:10.2118/129329-JPT.

Nierode, D.E., and Williams, B.B., "Characteristics of Acid Reactions in Limestone Formations," SPEJ, 306–314, 1972.

Qiu, X., Aidagulov G., Ghommem, M. et al. 2018. Experimental Investigation of Radial and Linear Acid Injection into Carbonates for Well Stimulation Operations. Paper presented at the SPE Kingdom of Saudi Arabia Annual Technical Symposium and Exhibition, Dammam, Saudi Arabia, 23–26 April. SPE-192261-MS. https://doi.org/10.2118/192261-MS.

Schwalbert, M. (2019, August 1). Comprehensive Analysis of Acid Stimulation in Carbonates. PhD Dissertation, Texas A&M University, College Station, TX.

Tardy, P. M. J., Lecerf, B., and Christanti, Y. 2007. An Experimentally Validated Wormhole Model for Self-Diverting and Conventional Acids in Carbonate Rocks under Radial Flow Conditions. Paper presented at the European Formation Damage Conferences, Scheveningen, The Netherlands, 30 May–1 June. SPE-107854-MS. https://doi.org/10.2118/107854-MS.

APPENDIX A

This Appendix section is to show the scale up calculations for the Schwalbert (2019) global wormhole model to determine the optimal interstitial velocity and pore volumes to breakthrough at field scale using results from linear core floods. The optimal interstitial velocity and pore volumes to breakthrough results from the Indiana Limestone core floods taken from the large block were 1.3 cm/min and 0.41 respectively. Both field scale parameters are calculated in a very similar manner with the equations for the scale up optimal interstitial velocity and pore volumes to breakthrough given as:

$$PV_{bt,opt} = PV_{bt,opt,core} f_1 \tag{21}$$

$$v_{i,opt} = v_{i,opt,core} f_2 \tag{22}$$

where $PV_{bt,opt}$ is the field scale pore volumes to breakthrough, $PV_{bt,opt,core}$ is the optimal pore volumes to breakthrough for the core flood, $v_{i,opt}$ is the field scale interstitial velocity in cm/min, $v_{i,opt,core}$ is the optimal interstitial velocity for the linear core flood in cm/min, f_1 is the scaling factor for the pore volumes to breakthrough, and f_2 is the scaling factor for the interstitial velocity. Mentioned in the literature review section, when applying this model to the field scale in radial acidizing, f_1 and f_2 can estimated using the shortened equation containing the representative values and is calculated as follows:

$$f_1 = (\frac{d_{core}}{59})^{\varepsilon_1} = (\frac{1.5}{59})^{0.53} = 0.143 \tag{23}$$

$$f_2 = (\frac{d_{core}}{34})^{\varepsilon_2} = (\frac{1.5}{34})^{0.63} = 0.140 \tag{24}$$

The scaled optimal interstitial velocity and pore volumes to breakthrough can now be calculated as:

$$PV_{bt,opt} = PV_{bt,opt,core} f_1 = (0.41)(0.143) = 0.059 \quad (25)$$

$$v_{i,opt} = v_{i,opt,core} f_2 = (1.3)(0.140) = 0.18\ cm/min \quad (26)$$

The calculated optimal values can now be used in Appendix B to determine the required flow rate to achieve these values.

APPENDIX B

Appendix B is dedicated to the calculations for determining the optimal injection conditions along with showing how the wormholes should theoretically propagate with time as given in the Schwalbert (2019) dissertation. From Appendix A, the scaled PV_{bt} is 0.059, and the scaled optimal interstitial velocity is given as 0.18 cm/min. Therefore, the f_1 and f_2 scaling factors for the following v_{wh} equation have already been applied and the equation will appear slightly different to the one found in the dissertation. As mentioned in the "Scale Up and Pumping Conditions" section, the flow rate will be selected in which the optimal interstitial velocity will be reached as close to breakthrough as possible. The equation for interstitial velocity in cm/min is given as

$$v_i = \frac{(1.075\ X\ 10^{-3})q}{2\pi h r_{wh}\varphi} \tag{27}$$

where q is the flow rate in mL/min, h is the completion height in ft, r_{wh} is the wormhole radius in ft, and φ is porosity. The wormhole velocity is given by

$$v_{wh} = \frac{\left(\frac{v_i}{PV_{bt,opt}}\right)\left(\frac{v_i}{v_{i,opt}}\right)^{-\gamma}\left\{1 - exp\left[-4\left(\frac{v_i}{v_{i,opt}}\right)^2\right]\right\}^2}{30.48} \tag{28}$$

where v_{wh} is in ft/min, $PV_{bt,opt}$ is the optimal pore volumes to breakthrough, and $v_{i,opt}$ is the optimal interstitial velocity in cm/min found from Appendix A. The radius of the wormhole, r_{wh}, can be calculated using the equation

$$(r_{wh})_{n+1} = (r_{wh})_n + v_{wh}\Delta t \tag{29}$$

where $(r_{wh})_{n+1}$ is the radius of the wormhole at the new time step in ft, $(r_{wh})_n$ is the wormhole radius at the current time in ft, Δt is the change in time in min, and v_{wh} is the wormhole velocity in ft/min. The easiest way to solve this system of equations is by using a time step, and

calculating each parameter for consecutive times starting when the radius of the wormhole is equal to the radius of the wellbore. The interstitial velocity will be calculated first, then that value will be plugged into the wormhole velocity equation, which will then be plugged into the wormhole radius growth equation. Then the process starts over with the new wormhole radius and time stamp. Two sets of calculations will be shown before the Microsoft Excel spreadsheet which contains the final time steps until breakthrough is reached.

Constants	
q	190 mL/min
h	1 foot
r_w	0.042 feet (0.5 inches)
φ	9.1%
$PV_{bt,opt}$	0.059
$v_{i,opt}$	0.18 cm/min
γ	1/3
Δt	0.2 min

Table 3. Constants for Appendix B calculations

For t=0 minutes,

Wormhole radius is given as r_w because wormholes have not propagated yet.

Interstitial velocity is given as:

$$v_i = \frac{(1.075\ X\ 10^{-3})q}{2\pi h r_{wh}\varphi} = \frac{(1.075\ X\ 10^{-3})(190)}{2\pi(1)(0.042)(0.091)} = 8.59\ cm/min \tag{30}$$

Wormhole velocity is given as:

$$v_{wh} = \frac{\left(\frac{v_i}{PV_{bt,opt}}\right)\left(\frac{v_i}{v_{i,opt}}\right)^{-\gamma}\left\{1 - exp\left[-4\left(\frac{v_i}{v_{i,opt}}\right)^2\right]\right\}^2}{30.48}$$

$$= \frac{\left(\frac{8.59}{0.059}\right)\left(\frac{8.59}{0.18}\right)^{-\frac{1}{3}}\left\{1 - exp\left[-4\left(\frac{8.59}{0.18}\right)^2\right]\right\}^2}{30.48} \tag{31}$$

$$= 1.33\frac{ft}{min}$$

The new wormhole radius for the next time stamp is given as:

$$(r_{wh})_{n+1} = (r_{wh})_n + v_{wh}\Delta t = 0.042 + (1.33)(0.2) = 0.31\ ft \tag{32}$$

For t=0.2 minutes,

Interstitial velocity is given as:

$$v_i = \frac{(1.075\ X\ 10^{-3})(190)}{2\pi(1)(0.31)(0.091)} = 1.16\ cm/min \tag{33}$$

Wormhole velocity is given as:

$$v_{wh} = \frac{\left(\frac{1.16}{0.059}\right)\left(\frac{1.16}{0.18}\right)^{-\frac{1}{3}}\left\{1 - exp\left[-4\left(\frac{1.16}{0.18}\right)^2\right]\right\}^2}{30.48} \tag{34}$$

$$= 0.35\frac{ft}{min}$$

New wormhole radius is given as:

$$(r_{wh})_{n+1} = 0.31 + (0.35)(0.2) = 0.38\ ft \tag{35}$$

The tabulated values from the excel spreadsheet are the following where the volume was calculated by multiplying the flow rate (190 mL/min) by time:

t [min]	v_i [cm/min]	v_{wh} [ft/min]	r_{wh} [ft]	V (L)
0.0	8.59	1.33	0.04	0.00
0.2	1.16	0.35	0.31	0.04
0.4	0.95	0.31	0.38	0.08
0.6	0.81	0.28	0.44	0.11
0.8	0.72	0.26	0.49	0.15
1.0	0.66	0.24	0.55	0.19
1.2	0.60	0.23	0.59	0.23
1.4	0.56	0.22	0.64	0.27
1.6	0.52	0.21	0.68	0.30
1.8	0.49	0.20	0.72	0.34
2.0	0.47	0.19	0.76	0.38
2.2	0.45	0.19	0.80	0.42
2.4	0.43	0.18	0.84	0.46
2.6	0.41	0.17	0.87	0.49
2.8	0.39	0.17	0.91	0.53
3.0	0.38	0.17	0.94	0.57
3.2	0.37	0.16	0.98	0.61
3.4	0.35	0.16	1.01	0.65
3.6	0.34	0.16	1.04	0.68
3.8	0.33	0.15	1.07	0.72
4.0	0.32	0.15	1.10	0.76
4.2	0.32	0.15	1.13	0.80
4.4	0.31	0.14	1.16	0.84
4.6	0.30	0.14	1.19	0.87
4.8	0.29	0.14	1.22	0.91
5.0	0.29	0.14	1.25	0.95
5.2	0.28	0.14	1.28	0.99
5.4	0.27	0.13	1.30	1.03
5.6	0.27	0.13	1.33	1.06
5.8	0.26	0.13	1.36	1.10
6.0	0.26	0.13	1.38	1.14
6.2	0.25	0.13	1.41	1.18

6.4	0.25	0.13	1.43	1.22
6.6	0.25	0.12	1.46	1.25
6.8	0.24	0.12	1.48	1.29
7.0	0.24	0.12	1.51	1.33
7.2	0.23	0.12	1.53	1.37
7.4	0.23	0.12	1.56	1.41
7.6	0.23	0.12	1.58	1.44
7.8	0.22	0.12	1.60	1.48
8.0	0.22	0.12	1.63	1.52
8.2	0.22	0.11	1.65	1.56
8.4	0.21	0.11	1.67	1.60
8.6	0.21	0.11	1.69	1.63
8.8	0.21	0.11	1.72	1.67
9.0	0.21	0.11	1.74	1.71
9.2	0.20	0.11	1.76	1.75
9.4	0.20	0.11	1.78	1.79
9.6	0.20	0.11	1.80	1.82
9.8	0.20	0.11	1.83	1.86
10.0	0.19	0.10	1.85	1.90
10.2	0.19	0.10	1.87	1.94
10.4	0.19	0.10	1.89	1.98
10.6	0.19	0.10	1.91	2.01
10.8	0.19	0.10	1.93	2.05
11.0	0.18	0.10	1.95	2.09
11.2	0.18	0.10	1.97	2.13
11.4	0.18	0.10	1.99	2.17
11.6	0.18	0.10	2.01	2.20

Table 4. Calculation results for wormhole growth

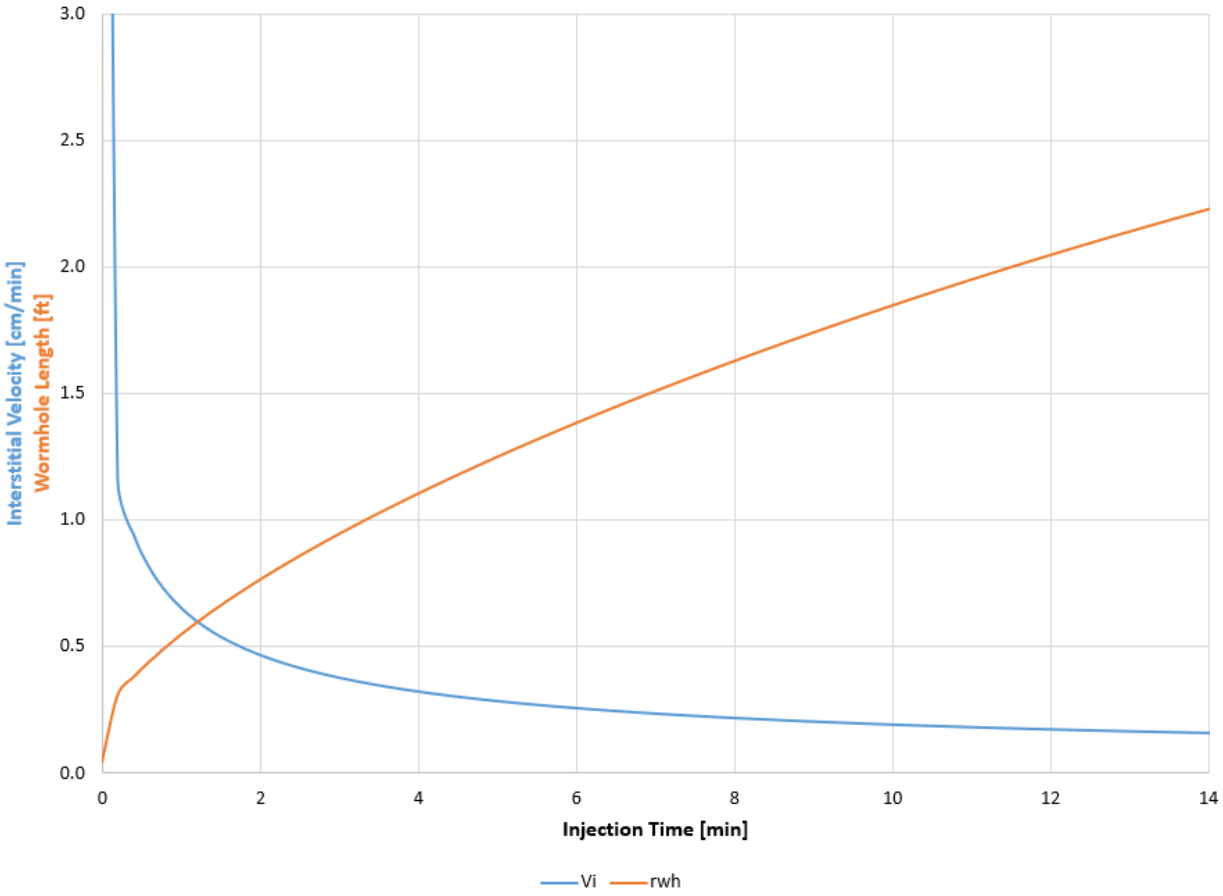

Figure 46. Theoretical breakthrough